energies

MDPI

Review

Hydrogen Production as a Clean Energy Carrier through Heterojunction Semiconductors for Environmental Remediation

Ashkan Bahadoran [1], Qinglei Liu [1,*], Seeram Ramakrishna [2], Behzad Sadeghi [3], Moara Marques De Castro [3] and Pasquale Daniele Cavaliere [4,*]

[1] State Key Laboratory of Metal Matrix Composite, Shanghai Jiao Tong University, Shanghai 200240, China; shayan@sjtu.edu.cn
[2] Faculty of Mechanical Engineering, National University of Singapore, Singapore 117574, Singapore; mpesr@nus.edu.sg (S.R.); moara.m.castro@gmail.com (M.M.D.C.)
[3] Centre of Excellence for Advanced Materials Application, Slovak Academy of Sciences, Dubravska Cesta 9, 84511 Bratislava, Slovakia; behzad.sadeghi@savba.sk
[4] Department of Innovation Engineering, University of Salento, Via per Arnesano, 73100 Lecce, Italy
* Correspondence: liuqinglei@sjtu.edu.cn (Q.L.); pasquale.cavaliere@unisalento.it (P.D.C.)

Abstract: Today, as a result of the advancement of technology and increasing environmental problems, the need for clean energy has considerably increased. In this regard, hydrogen, which is a clean and sustainable energy carrier with high energy density, is among the well-regarded and effective means to deliver and store energy, and can also be used for environmental remediation purposes. Renewable hydrogen energy carriers can successfully substitute fossil fuels and decrease carbon dioxide (CO_2) emissions and reduce the rate of global warming. Hydrogen generation from sustainable solar energy and water sources is an environmentally friendly resolution for growing global energy demands. Among various solar hydrogen production routes, semiconductor-based photocatalysis seems a promising scheme that is mainly performed using two kinds of homogeneous and heterogeneous methods, of which the latter is more advantageous. During semiconductor-based heterogeneous photocatalysis, a solid material is stimulated by exposure to light and generates an electron–hole pair that subsequently takes part in redox reactions leading to hydrogen production. This review paper tries to thoroughly introduce and discuss various semiconductor-based photocatalysis processes for environmental remediation with a specific focus on heterojunction semiconductors with the hope that it will pave the way for new designs with higher performance to protect the environment.

Keywords: semiconductors; photocatalysis; heterojunctions; environmental purification; composite photocatalysts

Citation: Bahadoran, A.; Liu, Q.; Ramakrishna, S.; Sadeghi, B.; De Castro, M.M.; Cavaliere, P.D. Hydrogen Production as a Clean Energy Carrier through Heterojunction Semiconductors for Environmental Remediation. *Energies* **2022**, *15*, 3222. https://doi.org/10.3390/en15093222

Academic Editor: Muhammad Aziz

Received: 27 March 2022
Accepted: 24 April 2022
Published: 28 April 2022

1. Introduction

1.1. Hydrogen as a Clean Energy Carrier

Today, as a result of the increasing population and the increasing need for clean resources due to environmental limitations, the search for sustainable and clean origins is becoming an increasingly crucial issue. Unfortunately, most of the energy requirement is mainly fulfilled by fossil fuels with finite reserves, and their consumption leads to the generation of greenhouse gases, leading to climate changes along with other significant adverse environmental issues. In this regard, renewables or alternative energy sources, such as solar, wind and biomass, were introduced to reduce greenhouse gases, especially carbon dioxide. Traditional energy production technologies account for an energy supply that is one order of magnitude higher than that from solar photovoltaic. The miniaturization of equipment allows rapid development because of lower investment costs and increased efficiency. Now, in many parts of the world, solar provides the cheapest electricity,

and the milestone of attaining a cumulative capacity of more than 1 TW is expected by 2023 [1]. Present integration strategies and those under development will provide extensive penetration of solar photovoltaics, not only in the power grid but also in the entire energy system.

Crucial transformation and a substantial renovation of the energy system in the world are required to decarbonize and attain the Paris Agreement targets. This significant reform is accompanied by an urgent and complex issue that needs system solutions and global joint and coordinated efforts, with hydrogen representing one of these solutions. Hydrogen is one of the key players in achieving a low-carbon energy system. It has the capability to be an influential accelerator for this system, with the ability to address multiple energy challenges, such as facilitating the vast integration of renewable resources and decarbonization of energy production, energy transportation in a zero-carbon energy economy, and electrification of end uses. Hydrogen is one of the most promising sustainable energy carriers that can be substituted for fossil fuels, and has a high gravimetric energy density ranging from 120 to 142 MJ/kg, compared to 44.5 MJ/kg for gasoline [2]. In addition, hydrogen combustion is clean (CO_2 free) and leads to water production ($2H_2 + O_2 \rightleftharpoons 2H_2O$; $\Delta E = -286$ kJ/mole). However, nearly 96% of hydrogen production is highly interdependent on fossil fuels; hence the need to find renewable resources is crucial. Recently, hydrogen has seen unprecedented interest and development. Soon, it will become a systemic element in the efforts to transition to a climate-neutral society, and, by replacing coal, oil, and gas, it will play the role of a crucial energy vector and the other leg of the energy transition—in addition to renewable electricity—across various parts of the economy.

The growing demand for renewable energy sources in the electricity sector has increased the need for supplementary technologies to balance the grid. However, electricity cannot be stored easily, which presents an opportunity for the application of hydrogen and the development of its technologies. Hydrogen technologies can play an influential role in energy distribution in order to provide conditions for reducing carbon consumption. Delivery has a crucial role in energy use, cost, and emissions, which are closely related to the available options of hydrogen delivery, including transportation via pipelines or road transport. This choice is dependent upon location, local geography, and markets. The combined use of renewable resources is important to the provision of constant power and the achievement of a stabilized electrical grid. Hydrogen can be converted back to electricity when other renewable sources are unavailable. Moreover, the excess can be sold for other purposes. In addition, hydrogen can be used as the primary feedstock of industries using fertilizer, refining, and other chemical-based technologies, and can also be a side product of other industrial processes, making it a strategically important commodity. It can be simultaneously injected into the natural gas grid to maintain a clean gas distribution by reducing emissions and other stranded assets. To stabilize electric grids, controlling the flow of electricity output from renewable energy power generators is crucial. Electricity storage facilities are required to make effective use of renewable energy and avoid output control. A key role in this matter for the immediate future is storage batteries. With the development of renewable energy, the urgency of output controls will also increment; however, hydrogen will also be used in large-scale and long-term power-to-gas systems. Renewable hydrogen can be used in many ways. It is the feedstock for producing methane, clean chemicals, and fertilizers. Hydrogen is considered to be fundamental in helping the value chain of different industries. Hydrogen can be obtained from natural gas reforming and/or pyrolysis, and transported through traditional pipelines mixed with methane. It is an energy carrier for many chemical transformations to be employed in industry such as ammonia. Ammonia (NH_3): (1) has a higher hydrogen density (1.5 times higher than liquefied hydrogen) than other carriers, its production needs cheaper infrastructure, and it can be developed through smaller-scale industries; (2) has easily available and existing commercial supply chains; (3) is produced from natural gas and relatively cheaper. Ammonia can be directly used for power generation without a need for the dehydrogenation process and emits no CO_2 during combustion. Hydrogen can be used for building heating as a fuel,

to leverage hydrogen technologies individually, or a combination of both, which offers high efficiency for heat and power generation. The handling of hydrogen as a fuel is similar to that of natural gas. Hydrogen can be combined with fuel cell technologies that generate electricity and heat to ultimately reduce carbon in several areas such as transportation, power generation, many kinds of industrial processes, and heat use. Natural gas power generation features are essential for the expansion of renewable energy power generation. Hydrogen power generation can be applied the same way as natural gas power generation and may become an outstanding option for reducing carbon in fossil power generation. Hydrogen can also be combined with CO_2 to produce methane, namely, the methanation process. There is extreme potential in methane serving as an energy carrier for the efficient usage of existing energy supply infrastructure (such as city gas pipes, liquefied natural gas power plants), and low-carbon heat use.

Using hydrogen power generation to provide value in electricity production as a regulated power supply source and increase generation capacity is expected. It seems that hydrogen power generation will play an effective role in decreasing carbon emissions and provide a regulated power supply and backup power source for extending renewable energy. Massive amounts of hydrogen will be consumed by hydrogen-based power generation, so its international supply chain development is very important. The cooperation of hydrogen with natural gas can be used in power generation systems. Initially, it will be used in existing natural gas power plants and in small-scale cogeneration systems to promote hydrogen diffusion. Another significant aspect is related to its long-term electricity storage for utilization in massive renewable energy oversupply without output control. Hydrogen will play an effective role in energy storage, especially in large-scale systems and on a long-term basis over multiple seasons. Therefore, hydrogen will have a significant impact and act as a key player in renewable energy in order to reduce carbon amounts in the electricity system. Further developments will lead us to use hydrogen in large-scale energy storage, transportation fuel, and power-to-gas applications, thus providing a clean and viable energy source that can be used for vehicles, households, larger buildings, etc. Additionally, hydrogen derived from seawater is a potentially game-changing solution and is heralded as an enabler of the Grand Transition into a cleaner future [3].

1.2. Hydrogen from Semiconductor-Based Photocatalysis

Concerning the clean production of hydrogen, semiconductor-based photocatalysis seems to be a promising scheme. Hydrogen production through photocatalysis processes is similar to that of photovoltaic systems via the utilization of semiconductor materials such as TiO_2 [4]. The catalysis process according to the phase distribution of catalysts, reagents, and products, can be categorized into two kinds, homogeneous and heterogeneous; however, due to its ease of separation, heterogeneous catalysis is more preferred. A kind of heterogeneous catalysis that utilizes photon energy is known as semiconductor-based photocatalysis, in which a solid material is stimulated by exposure to light and generates an electron–hole pair. Subsequently, the photogenerated species take part in redox reactions. The first inspirational introduction of the photoelectrochemical cell dates back to 1972 by Honda and Fujishima, in which the water was split into oxygen and hydrogen using ultraviolet (UV) irradiation [5]; since then, many studies have focused on the development and improvement of the photocatalysis process.

In these processes, the photogenerated carriers should migrate to the surface of the photocatalysts to engage in necessary electrochemical reactions. One of the most important challenges is the recombination of photogenerated charge carriers (electrons and holes), which, unfortunately, is preferable in terms of thermodynamic energy. This negatively impacts photocatalysis performance since a small number of photogenerated species can find a chance to migrate to the surface of the catalysts and become involved in redox reactions. Several strategies have been introduced to overcome the electron–hole recombination issue, including the inclusion of noble-metal co-catalysts [6,7], cation/anion doping [8,9], and the

fabrication of heterojunctions between different semiconductors, which is also referred to as composite photocatalysis [10,11].

Hierarchically ordered macro-mesoporous TiO_2-graphene composite films show the enriched capacity of quickly adsorbing and photodegrading organic dyes. The assembling of interconnected macropores in mesoporous films has the following effects: (1) improves the mass transport through the film; (2) increases the accessible surface area of the thin film; (3) significantly enhances their photocatalytic activities; and (4) reduces the length of the mesopore channel. These structures are potentially suitable for wastewater treatment and air purification for removing organic pollutants and will provide an attractive opportunity for industrial applications.

Photocatalytic processes have the potential to develop renewable and eco-friendly energy carriers such as H_2 and O_2 by water splitting [12,13]; they can also degrade various organic pollutants [14–18], convert energy conversion, be used in material storage by photocatalytic CO_2 reduction [19–21], synthesize organic substances [14,22,23], and even reduce iron ore with hydrogen [24]. In this regard, both energy issues and environmental pollution treatment can be economically solved by semiconductor-mediated photocatalysis procedures, and hydrogen, as an ideal green fuel, can be produced through the photocatalytic reduction of protons by the photoinduced electrons; hence, toxic organic pollutants can be degraded by utilization of multi-step photocatalytic oxidation reactions [25]. Unfortunately, a single semiconductor cannot lead to quick recombination of photoinduced charge carriers because of the extensive exciton binding energy [26,27]. Therefore, the fabrication of heterostructure photocatalysts, well-designed heterojunctions, and multi-component semiconductors is of eminent importance to maintain simultaneous extended light-harvesting range, efficient interfacial charge separation, and high redox potential. It was proven that realistic and intelligent selection of semiconductors and tailoring of well-suited energy band structures for the production of heterojunction photocatalysts should be fully considered to fulfill the above-mentioned factors [28–30]. Until now, numerous strategies have been introduced to improve the photocatalytic performance of semiconductors for efficient hydrogen production, including homogenous and heterogenous methods, S-scheme, Z-scheme, and artificial photocatalysis [31].

Among these existing strategies, it seems that heterojunctions that use two semiconductors to reduce the recombination rate and simplify the migration of photogenerated species towards the surface are an emerging scheme to design novel photocatalysis systems. The heterojunctions are usually fabricated by two or more semiconductors and have coordinated energy bands; they were proven to have exceptional efficiency for improving photocatalytic activity, mainly due to spatially separated photogenerated electron–hole pairs at the heterojunctions' interface [32]. Furthermore, visible-light driven heterojunction photocatalysts, due to their ecofriendly nature, are more preferred by the community. It is believed that photocatalytic hydrogen fabrication, organic pollution treatment, and heavy metal reduction by utilization of various types and schemes of heterostructure photocatalysts will remain and continue to progress as a significant and practical topic in the coming decades [33].

In this regard, this review paper is devoted to thoroughly introducing and discussing various semiconductor-based photocatalysis processes for environmental remediation, with a specific focus on heterojunction semiconductors in order to find an efficient means of designing novel photocatalysis systems with high throughput performances. Additionally, the related photocatalytic performance of various structures and the positions of energy bands are explained and summarized to maintain a direct view. The influential factors in achieving the maximized performance, the applications, the conventional and modern techniques, the improvements, and any key and minor factors that play a role in the effective hydrogen production by heterojunction-based semiconductors photocatalysis were studied. This review paper, for the first time, briefly gathers all the information about eco-friendly hydrogen generation from heterojunction-based semiconductor photocatalysis

for environmental remediation and energy harvesting, and can lead specialists to design more novel schemes with high throughput performances.

2. Materials and Methods

Based on the electrical conductivity, materials can be categorized into conductors, semiconductors, or insulators. Conductor materials have a high electrical conductivity in the range of 10^7 Ωm^{-1}, whereas insulators have low conductivity in the order of 10^{10} Ωm^{-1}. Semiconductors are located between the other two groups, having electrical conductivity in the range of 10^{-6} to 10^4 Ωm^{-1}; this difference in conductivity originates from the energy bands. Electrons reside in specific bands, in which the lower energy valence band includes valence electrons, whereas the higher energy position is entitled the conduction band and is empty in the ground state. The energy variance between these two energy bands is known as the bandgap, and the bandgap energy (E_g) corresponds to its magnitude. It should be noted that the electrons located between conduction and valence band energy levels cannot exit, and conduction occurs due to the movement of free electrons in the conduction band above the Fermi level. In conductor materials, the Fermi level lies in the overlapping region of the conduction and valence bands, as shown in Figure 1 [34,35]. In contrast, insulators and semiconductors have a bandgap between the valence and the conduction bands in which the Fermi level lies. Electrons can be excited to the conduction band by absorbing higher energies than the bandgap. The bandgap of semiconductor materials is narrower than that of insulators. If an electron (e^-) is promoted to the conduction band from the valence band, one hole (h^+) is generated in the valence band. The interaction between these electrons and holes leads to conductivity in semiconductors [36].

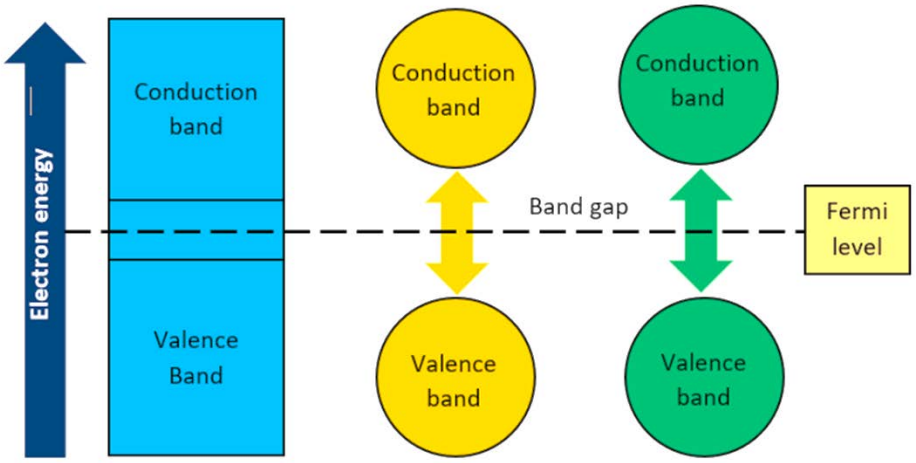

Figure 1. The difference between the band structures of conductors (metals), semiconductors, and insulators.

2.1. Semiconductor Photocatalysis

Semiconductor stimulation by photons with energies higher or equal to the semiconductor's bandgap (E_g) leads to the promotion of an electron (e^-) from the valence band (VB) to the conduction band (CB), generating a hole (h^+). Both the excited state in the conduction band and holes in the valence band are thermodynamically and kinetically prone to recombine and spend the input energy through heat generation or light emission, as illustrated in Figure 2a [37]. By comparison, if electrons and holes migrate to the semiconductor's surface without recombination, they can actively operate in electrochemical processes with species absorbed at the semiconductor surface. In this condition, photogenerated electrons act as reducing agents, and holes act as oxidizing agents. This redox capability of electron–hole pairs can be utilized in photocatalytic processes such as water/air remediation and hydrogen production.

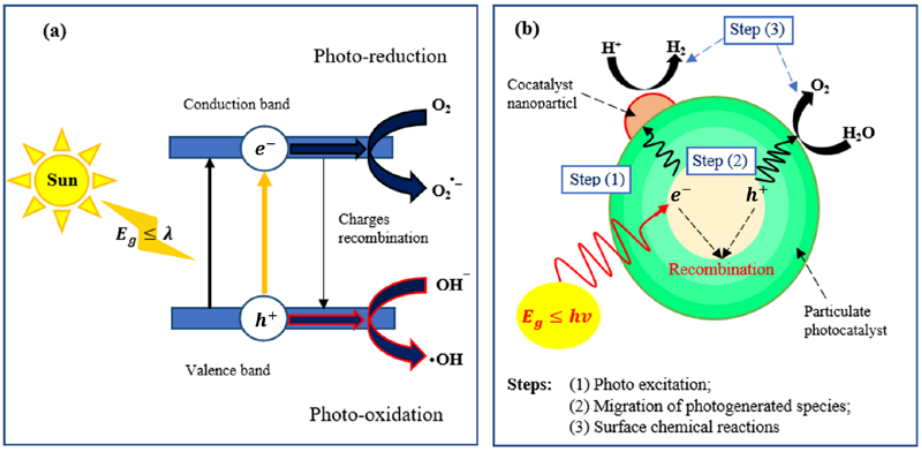

Figure 2. Photocatalytic reactions in semiconductors: (**a**) photocatalysis process and (**b**) three basic steps of photocatalysis in semiconductors.

Photocatalytic reactions in semiconductors have three basic steps, as shown in Figure 2b [38]: (1) photon excitation, (2) migration of photogenerated species, and (3) surface chemical reactions. In these processes, both electrons and holes play a crucial role; photogenerated electrons play a substantial role in water reduction while holes assist in the oxidative decomposition of environmental pollutants. These photocatalytic reactions, via the cooperation of electrons and holes, lead to hydrogen production and CO_2 reduction to fabricate further reduced carbon species such as CO or methanol.

2.2. Semiconductor Heterojunctions

Heterojunctions are generated at the interface between different semiconductors, and they are utilized in the case of unequal bandgaps, discontinuities in the bandgap, or the existence of an abrupt barrier in a specific band [39], as shown in Figure 3.

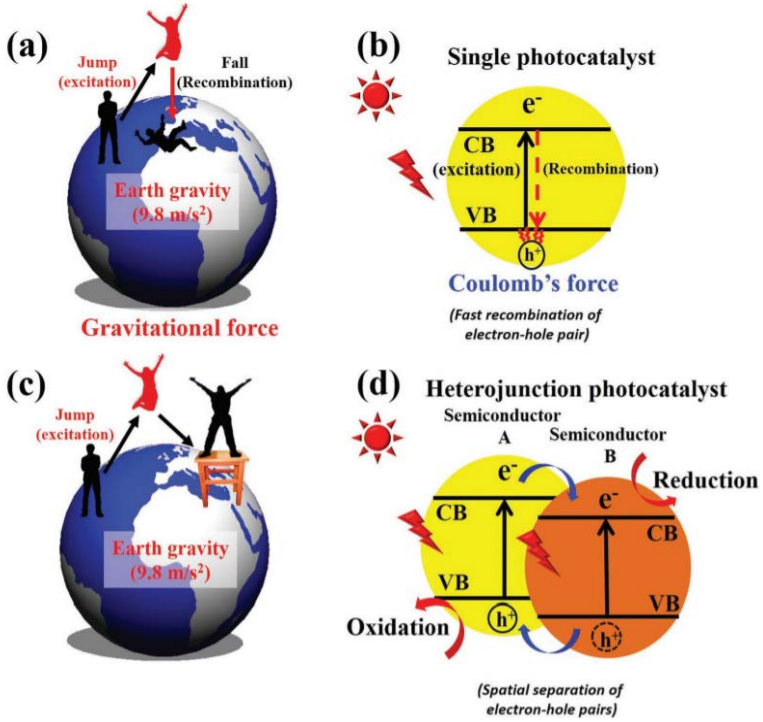

Figure 3. Illustration of: (**a**) the gravitational force effect on a jumping man; (**b**) electron–hole recombination on a single photocatalyst; (**c**) keeping a man off the ground using a stool; and (**d**) electron–hole separation on a heterojunction photocatalyst, adapted from [39].

When the electron (the man in Figure 3a) jumps from the valence band (the ground in Figure 3a) into the conduction band (the sky in Figure 3a), it must immediately recombine with a hole (the ground in Figure 3a) because of Coulomb attraction between the electron and the hole (the gravity of the Earth). Thus, in order to separate the electron–hole pairs that are photogenerated (keeping the man off the ground), the employment of a semiconductor B is needed (Figure 3c,d) and the electron and hole pairs remain separated. The composite photocatalyst or heterojunction has been designed to solve the issues of maximum charge carrier recombination along with the minimum visible-light activity. Heterojunctions with proper design can considerably improve the separation of photogenerated electron–hole pairs; hence, they can readily move to the surface to become involved in subsequent electrochemical reactions [40], as illustrated in Figure 4.

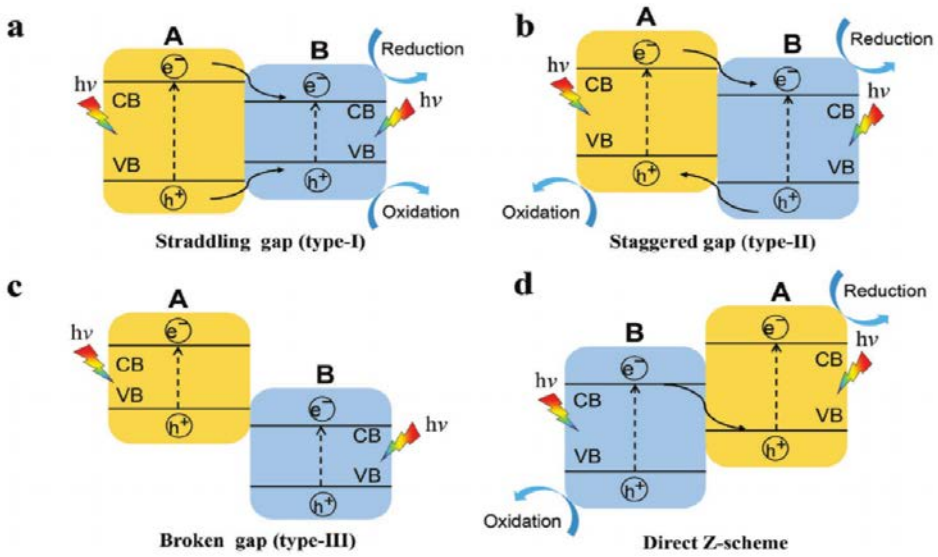

Figure 4. The electron–hole pairs' migration under irradiation in various type of heterojunction photocatalysts: (**a**) type-I, (**b**) type-II, (**c**) type-III, and (**d**) direct Z-scheme, adapted from [40].

The unique physical and special chemical properties of 2D semiconductors make them an ideal option for fundamental photocatalytic research and potential commercial applications. Heterojunctions employment allows for the extension of the light adsorption interval, for the efficient separation of the carriers of energy that are produced, and for the improvement in the photocatalytic activity. Here, the specific design of heterojunctions is fundamental to the optimization of components' functionalities and to the improvement of any synergic effect. As a matter of fact, 0D configurations allow for the activation of more active sites and the reduction in the migration distances of the charges. They can be designed using a structure having very versatile tunable bands in order to increase the catalytic activity. One-dimensional configurations act as very efficient charge transport from a ballistic point of view. In addition, one of their main actions is the suppression of potential agglomeration of 2D materials. The combination of 2D/2D heterojunctions allows for the increase in contact areas by increasing the charge transfer efficiency. Three-dimensional configurations allow for the increase in the efficiency of energy utilization by improving the transportation of the reacting compounds to the reaction sites. In addition, many improved properties can be obtained through the combination of different configurations, such as 2D/0D, 2D/1D, 2D/2D, and 2D/3D, by increasing the range of photocatalytic activities. Heterojunctions fabricated by two different semiconductors can be categorized into two major groups, known as p-n and non-p-n heterojunctions.

The Effect of Morphology in Heterojunctions

The morphology and structure of heterojunctions can substantially influence the activity of catalysts. In addition, the dimension and configuration can also affect the performance

of heterojunction photocatalysts. It was shown that two-dimensional (2D) materials are among the proper candidates for photocatalysis applications because of their favorable structural and electronic properties, but they still need to be improved because of disadvantages such as electron–hole recombination and low redox ability. In this regard, wise and objective construction of 2D heterojunction photocatalysts with various arrangements and morphologies can improve the photocatalytic activity [41]; Figure 5 shows the design of proficient 2D heterojunction photocatalysts with differing configurations, applications, and properties, each of which has its advantages and disadvantages.

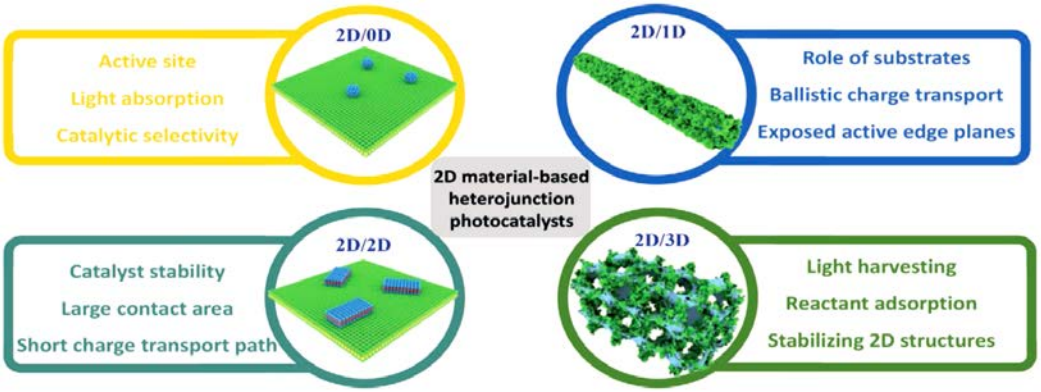

Figure 5. The schematic illustration of 2D heterojunction photocatalysts with various configurations, applications, and properties, adapted from [41].

Zhu et al. [42] investigated the impact of Bi_2WO_6 morphology on photocatalytic degradation of volatile organic compounds under visible light. They fabricated four types of Bi_2WO_6 morphologies (nest-like or flower-like) through the facile hydrothermal method, including BWO^{-1}, BWO^{-2}, BWO^{-3}, and BWO^{-4} with varying additives, synthesis temperature, time, and pH, as shown in Figure 6. It was shown that the nest-like Bi_2WO_6 structure manifested the most reaction active sites, leading to a 100% gaseous toluene degradation during only 20 min under visible-light irradiation. These abundant reaction active sites in the nest-like structure are due to their fine particle size, large photoresponse interval, narrow bandgap, improved electron–hole pair separation efficiency, and low electron–hole recombination rate, as shown in Figure 7 [42]. It was also shown that the double-shell Bi_2O_3/Bi_2WO_6 hollow microspheres demonstrated an improved photocatalytic activity because of the hollow presence in the structure and fabrication of the p−n junction between p-type Bi_2O_3 and n-type Bi_2WO_6 [43].

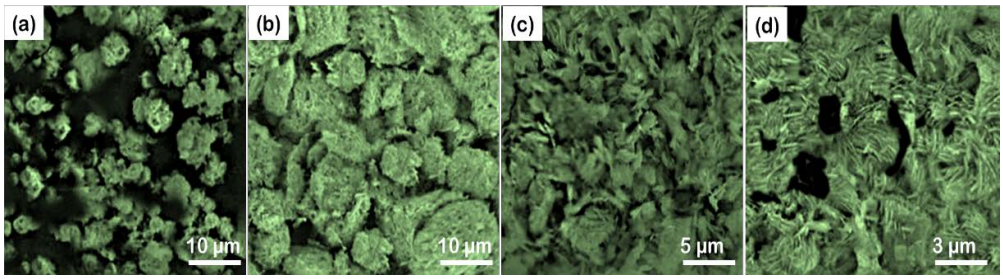

Figure 6. SEM micrographs showing (**a**) BWO^{-1}, (**b**) BWO^{-2}, (**c**) BWO^{-3}, and (**d**) BWO^{-4}.

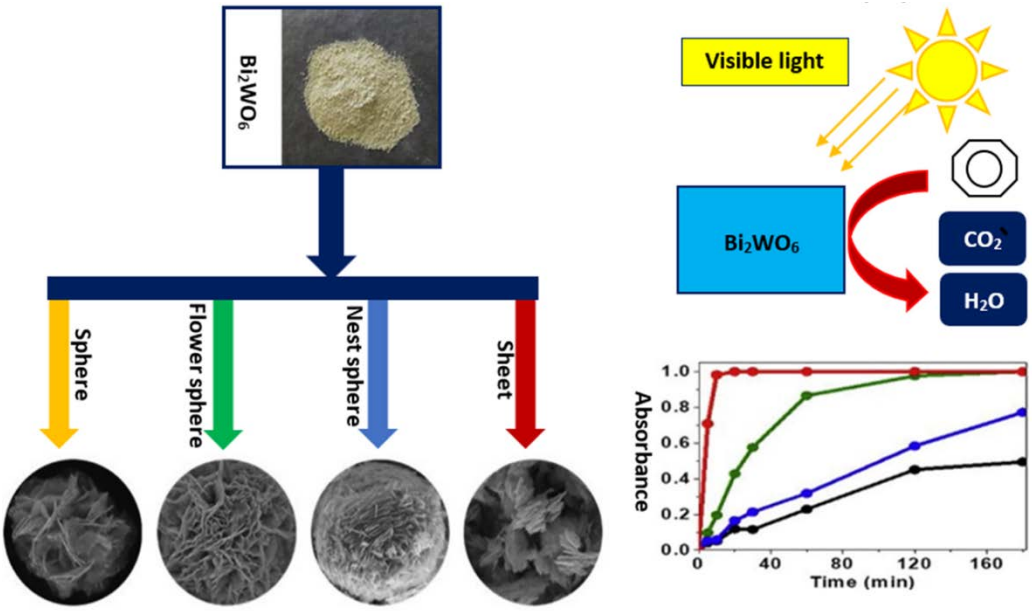

Figure 7. The morphology-dependent nature of Bi_2WO_6 photocatalysts on the degradation of volatile organic compounds under visible light.

For instance, Farhadian et al. [43] proved that morphology has a considerable influence on the photocatalytic activity of WO_3 nanostructures. They assessed three different morphologies, including nanoplate, nanosphere, and nanorods (as shown in Figure 8), in terms of their photocatalytic performance toward decomposition of rhodamine B (RhB) dye, proving that nanoplate WO_3 has the best photocatalytic activity. This improved performance of nanoplates is due to the sharp edges and corners of WO_3 nanoplates; hence, due to their low coordination number, the atoms in the edge and corner regions of the WO_3 nanoplates possess more activity in comparison to other morphologies and can adsorb more RhB, leading to more photocatalytic activity [43].

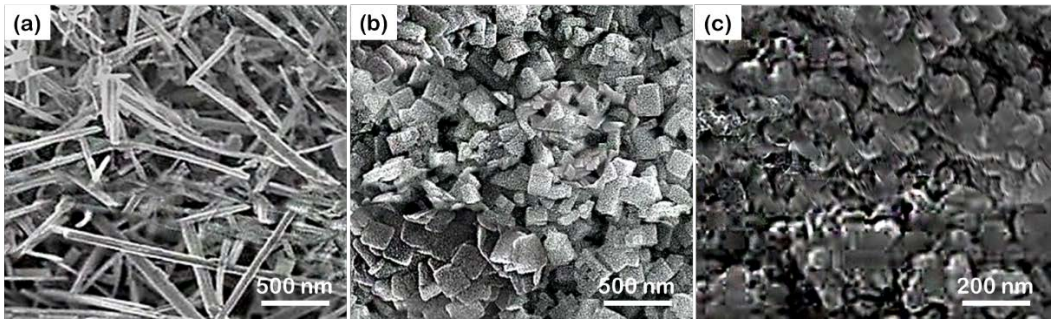

Figure 8. SEM micrographs showing the various morphologies of WO_3 photocatalysts: (**a**) nanoplates, (**b**) nanorods, and (**c**) nanospheres.

In a recent study, it was shown that the porous Ag/ZnO nanosheets with 3D self-assembled architecture act as a super photocatalyst for excellent organic pollutant degradation and hydrogen evolution [44–46], as schematically illustrated in Figure 9. These 3D porous structures are manufactured by a facile method following topological morphology evolution with low-temperature calcination. They showed highly photocatalytic activity with about complete degradation of 10 ppm 4-nitrophenol after just 25 min and a ~0.45 mmol g^{-1} h^{-1} hydrogen production rate [45]. The achieved excellent photocatalytic activity can be related to the morphological synergetic influence among 2D ZnO porous single-crystalline nanosheets and sliver species, and large surface area, improving separation and migration performance of charge carries and charge-collection efficiency [45].

In addition to morphology and structurally related factors, the defects can also influence the hydrogen production via heterojunction structures. Jing et al. [47] reported that the discrete defect energy-level introduction and reduction in the effective electrons' mass can improve the separation and migration procedures of the photoinduced charge carriers in the $ZnIn_2S_4$ microflowers. This one-step hydrothermal strategy, via the introduction of S-defect-controlled $ZnIn_2S_4$ microflowers, can effectively regulate the lattice defects of 2D sulfide semiconductors in the high throughput photocatalytic solar-to-fuel conversion [47].

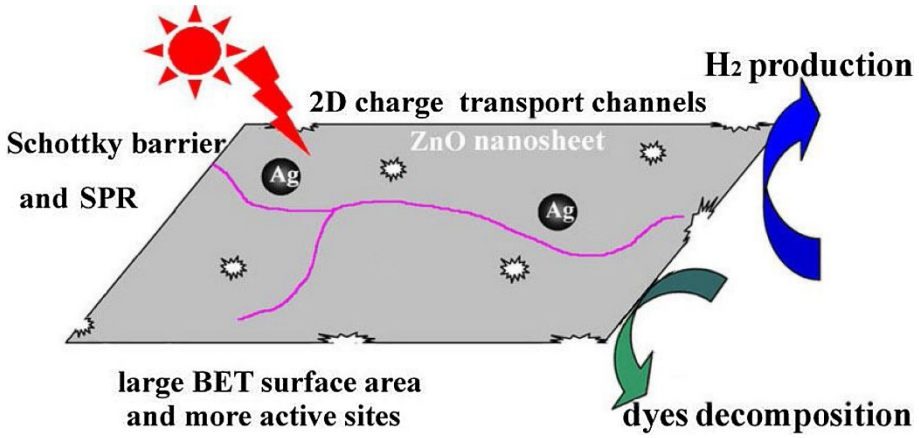

Figure 9. The architecture of Ag/ZnO and its photocatalytic mechanism, adapted from [44].

2.3. p-n Heterojunctions

In this type of heterojunction, two contacting semiconductors generate a p-n junction with a unique charge zone, enabling it to transmit electrons and holes in the reversed direction, as illustrated in Figure 10. In this regard, holes are transmitted to the VB region of the p-type semiconductor, while electrons are transmitted to the CB region of the n-type semiconductor. The driving force for this electron–hole transfer is the electric field generated inside the space charge region (junction). During the exposure of p–n heterojunction to photons with equal or higher bandgap energies than those of the photocatalysts, the photogenerated electron–hole pairs can be separated instantly due to the formed electric field in the space charge region. In this condition, the holes are moved to the VB zone of the p-type and the electrons are transferred to the CB region of the n-type semiconductors. This type of p-n semiconductor has many advantages, including (i) very effective charge separation; (ii) accelerated charge transfer; (iii) increased charge carriers' lifetime; and (iv) a regional separation of incompatible redox reactions in nano space [48].

According to the donor and acceptor characteristics, all semiconducting materials can be regarded either as a p- or n-type. If the p- and n-type semiconductors are coupled as shown in Figure 10 with suitable band gaps and band positions, they fabricate a form of p-n heterojunction composite. There are numerous varieties of p-n heterojunctions utilized in photocatalyst semiconductors, such as Cu_2O-TiO_2, NiO-TiO_2, NiO-ZnO, CuO-ZnO, CuO-$BiVO_4$, Bi_2O_3-Bi_2WO_6, and $CaFe_2O_4$-ZnO. It should be noted that the synthesis method is a crucial stage, and has a substantial impact on the mechanism and overall performance.

Photocatalytic decontamination is a promising procedure for environmental protection, with the ability to oxidize and mineralize numerous organic contaminants. Zinc oxide (ZnO), because of its favorable photoactivity, stability, availability, and nontoxic nature, is among the most interesting photocatalysts [48]. Unfortunately, ZnO suffers from a very poor response to visible light and unfavorable recombination of photogenerated species; thus, the constructing heterojunctions having the suitable band edges can substantially overcome the ZnO shortcomings and improve its photocatalytic performance. It was reported that ZnO-based binary and multiple heterojunction/nanocomposite photocatalysts, such as hydrothermally fabricated ZnO/CuO heterostructures, exhibit the best photocatalytic activity [49], as shown in Figure 11.

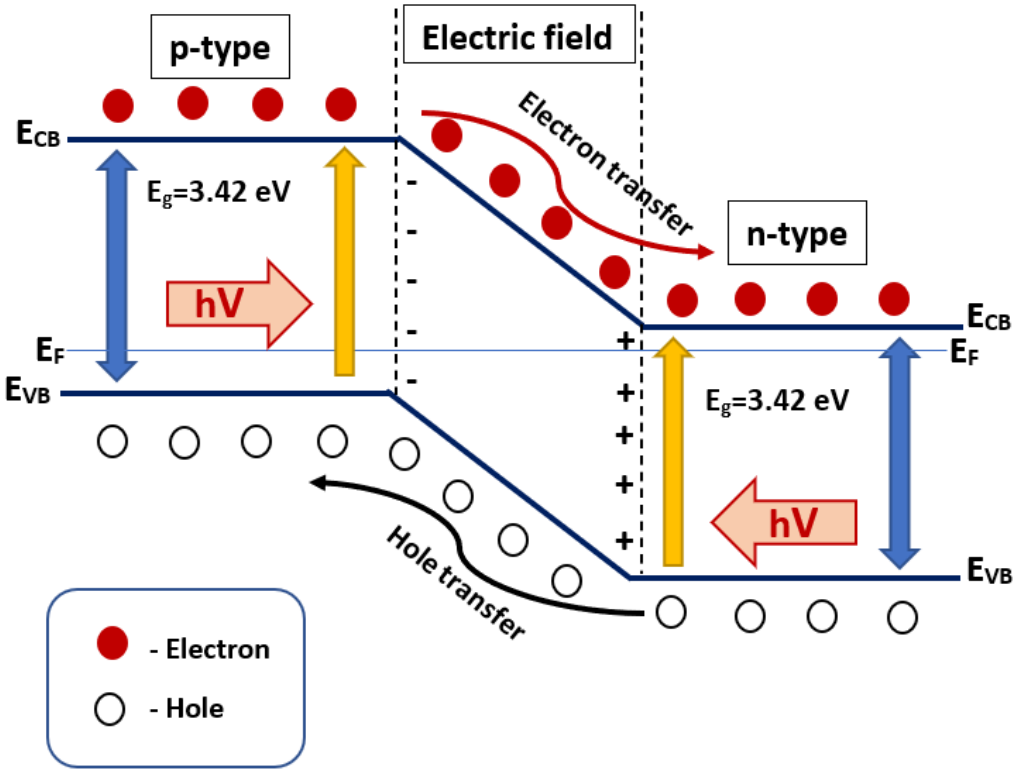

Figure 10. Schematic of p-n heterojunctions illustrating the energy band condition and separation of electron–hole pair.

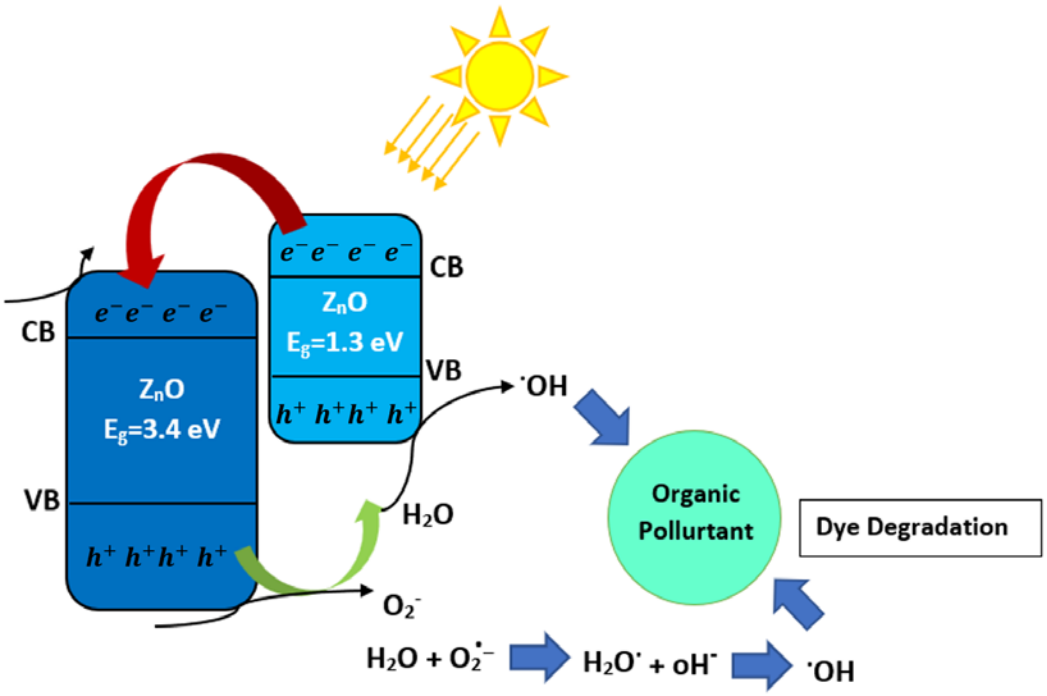

Figure 11. Schematic of a photocatalytic mechanism of ZnO/CuO heterojunction.

Accordingly, Habibi-Yangjeh et al. [50] synthesized a p-n heterojunction with ZnO/$ZnBi_2O_4$ nanocomposite to fabricate a durable visible-light-activated photocatalyst for organic pollutant degradation. The ZnO/$ZnBi_2O_4$ p-n heterojunction exhibits considerable photocatalytic ability compared to ZnO, with high throughput performance in the degradation of different pollutants. It should be mentioned that, in addition to photocatalytic applications of ZnO, it can also be

used for antibacterial improvements due to toxicity mechanisms in ZnO, including Zn^{2+} release, reactive oxygen species (ROS) generation, membrane dysfunction, and nanoparticle internalization into cells [51]. Although ZnO is considered one of the most traditional photocatalysts, numerous studies must be conducted for its improvement, particularly to enhance its visible-light response via bandgap narrowing. These include integration of ZnO with metallic and/or nonmetallic dopants, polymeric fabrications, dyes, and/or small bandgap semiconductors; heterojunction production between two or more semiconductors; and designing hierarchically structured photocatalysts with exposed reactive facets, as shown in Figure 12 [52].

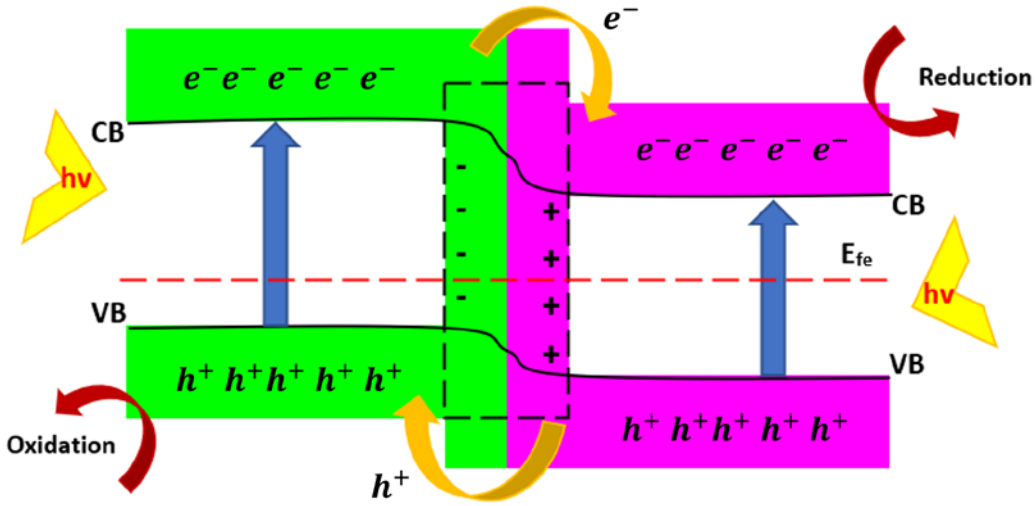

Figure 12. A simplified illustration of a p–n heterojunction construction.

Photocatalytic activity alongside photocatalytic recyclability of ZnO can be improved by the utilization of magnetic semiconductor materials. In the literature, numerous choices can be found for heterojunction construction, expanding the potential application of ZnO photocatalysts in practice, specifically in the environmental fields. A comprehensive study is required to investigate the variations in the electronic and lattice structure of the modified ZnO when it is doped/loaded with charged/uncharged elements and small bandgap semiconductors. In order to further comprehend the involved mechanism during photocatalytic reactions and construct efficient photoreactors, a modeling study is required for practical purposes.

2.4. Non p-n Heterojunctions

Non-p-n heterojunctions are made by tightly combining two or more semiconductors with relevant bandgap energies and band positions. These combined semiconductors must have very intimate contact to ensure and facilitate the photogenerated electron–hole pair transfer. In p-n junctions, there is a depletion region and the electric field for charge transfer, whereas in non-p-n junctions there are nano-scale junctions with photo-carrier collections occurring in in-band offsets. The visible-light-active heterojunctions that are generated by two semiconductors are categorized into four main groups based on the bandgaps and band position, namely, Type **I**: heterojunctions fabricated by visible-light-active and UV-active components; Type **II**: heterojunctions that are produced from two visible-light-active components; Type **III**: heterojunctions with Z-scheme; and Type **IV**: heterojunctions with the S-scheme mechanism.

2.4.1. Type I: Heterojunctions Made by Visible-Light-Active and UV-Light-Active Components

In this kind of heterojunction, just one of the components is active and able to fabricate electron–hole pairs under visible-light irradiation, whereas the second component cannot

produce photogenerated carriers. In this condition, the CB electrons of one component with a low bandgap energy can be transferred to the CB of the other component with high bandgap energy, and leave the hole in the VB of the exciting component. Subsequently, electrons can interact in surface chemical reactions, as shown in Figure 13. It must be mentioned that the conduction band position of the low bandgap semiconductor must be above that of the high bandgap component. This kind of heterojunction is used to broaden the absorption range of UV light active semiconductors toward visible light.

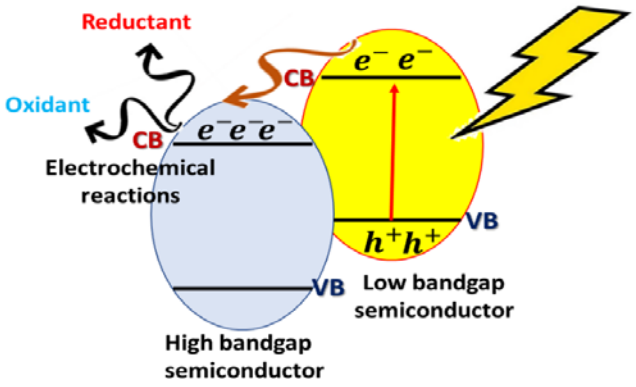

Figure 13. Schematic illustrating the heterojunctions produced from one visible-light-active component and other UV-light-active component.

There are numerous chalcogenide-contained heterojunctions in Type I semiconductors such as CdS-ZnO, ZnS-ZnO, CdS-TiO_2, CdS-Ta_2O_5, ZnSe-TiO_2-xNx, ZnSe-ZnO, and CdS-$NaNbO_3$. Some other heterojunctions of this group contain two semiconductor oxides, one with visible-light activity and the other UV light activities, such as In_2O_3-$Gd_2Ti_2O_7$, In_2O_3-TiO_2, In_2O_3-Ta_2O_5, $Gd_2Ti_2O_7$/$GdCrO_3$, $CaWO_4$/Bi_2WO_6, Bi_2O_3-Ag_3PO_4, Bi_2O_3-TiO_2, and Bi_2MoO_6-TiO_2. In this type of semiconductor, because photogenerated charge carriers must have easy mobility from one to another, the crystal structure has a crucial effect on charge separation [53]. It was also reported that $BiIO_4$/$BiVO_4$ heterojunction demonstrates the enhanced photoelectrochemical performance toward rhodamine B (RhB) degradation and photocurrent generation compared to the two individuals under visible light. Indeed, the promoted photocatalytic activity was related to the fabrication of a $BiIO_4$/$BiVO_4$ heterojunction since it provides an efficient interfacial charge transfer. Regarding the CdS-based materials, an electron-donating strategy can be utilized to improve the structure of metal-organic framework photocatalysts with a co-catalyst-free design for highly effective photocatalytic hydrogen evolution. In this regard, Dong et al. [54] designed an innovative CdS-based metal-organic framework photocatalyst with the cooperation of triethanolamine as the hole-scavenger, which eventually led to a very excellent Hydrogen evolution rate [54].

2.4.2. Type II: Heterojunctions Made by Two Visible-Light-Active Components

Type II heterojunctions are composed of two components that are both active in visible light and equally contribute to absorption, electron–hole pair separation, and electrochemical surface reactions. In order to work appropriately, the VB and CB of one component should be higher than the VB and CB of the other. Hence, the excited electrons can transfer to the CB of the other, while the photogenerated holes can transfer to the VB of the second, thus leading to an effective charge separation.

Until now, several heterojunctions from Type II have been introduced and investigated, such as a semiconductor containing graphitic carbon nitride (g-C_3N_4). Due to their small bandgap and layered structure, these semiconductors have promoted charge carrier portability and maximized charge carrier separation under visible light. Some of these graphitic carbon nitride semiconductors are graphene-g-C_3N_4, g-C_3N_4-BiOBr, g-C_3N_4-CdS, In_2O_3-g-C_3N_4, g-C_3N_4-Ag_3PO_4, g-C_3N_4-Bi_2WO_6, and g-C_3N_4-TaON. Some of the other members of this group are bismuth-based composite catalysts, such as BiOCl-Bi_2O_3,

Bi_2O_3-WO_3, WO_3-Bi_2WO_6, and Bi_2S_3-Bi_2WO_6. It should be noted that tungsten oxide (WO_3) is a proper semiconductor candidate due to its substantial visible-light absorption (≥480 nm), exceptional optical properties, and adjustable bandgap. In addition, WO_3 is highly beneficial because of its nontoxic and safe nature, economic cost, and durability in acidic and oxidative circumstances. The organic dye degradation by the WO_3/Ag_3PO_4 heterojunction semiconductor and the related mechanism is shown in Figure 14 [55].

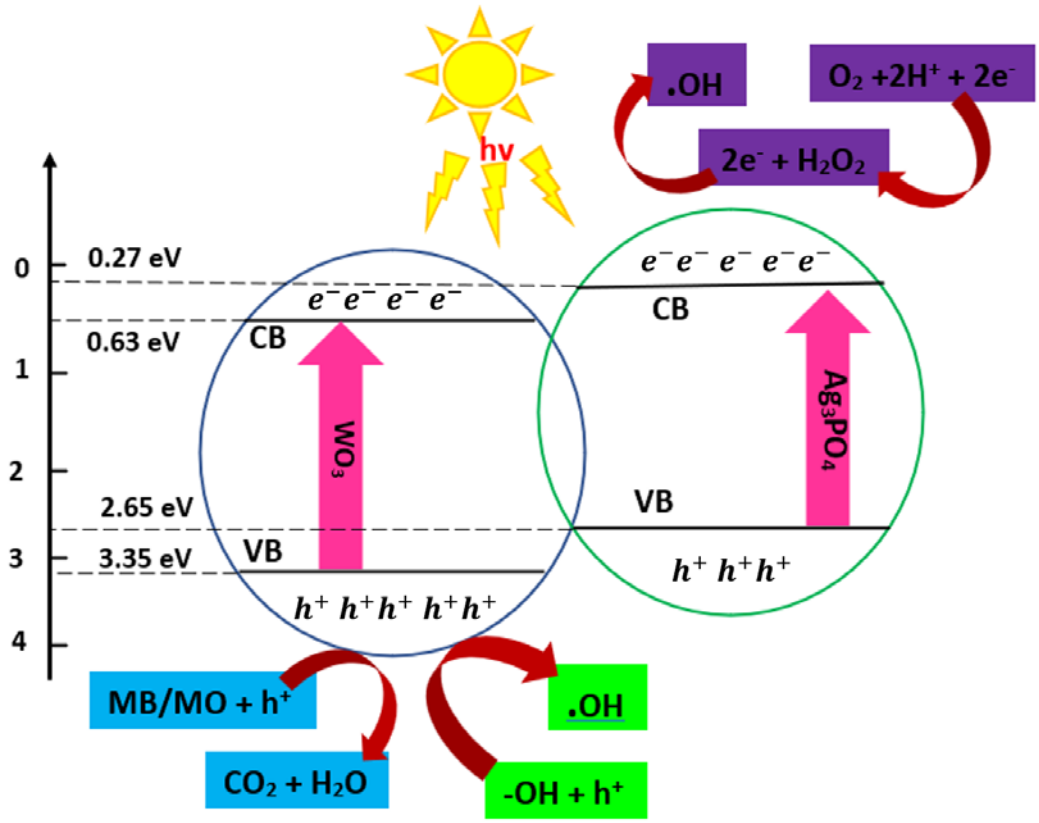

Figure 14. The organic dye degradation by the WO_3/Ag_3PO_4 heterojunction semiconductor and the related mechanism.

A small bandgap, nontoxicity, and high durability are some merits of WO_3 that cause favorable applications of WO_3 in photocatalysis. The improved catalytic activity was associated with high surface areas, separation capability, and the considerable charge transfers of WO_3 nanocomposites, and successfully transfers active sites and accelerates photogenerated charge transfer and separation. In addition, a proper scheme to increase photoinduced charge separation efficiency and its catalytic behavior is the formation of composites.

2.4.3. Type III: Heterojunctions with Z-Scheme Mechanism

Type III heterojunctions, like those of Type II, have two visible-light-active components, based on what is mentioned as the Z-scheme type. The natural photosynthesis (NPS) procedure in green plants converts the H_2O and CO_2 into O_2 and carbohydrates with the Z shape photosystem, as shown in Figure 15 [56]; this Z-scheme has a two-step photoexcitation process. In the same manner, the synthetic Z-scheme systems that try to mimic natural systems also consist of two connected semiconductor photocatalysts that can keep the electron–hole pairs with proper reduction/oxidation abilities on active regions [57]. In this type, the band positions located similarly to photogenerated holes in the VB of semiconductor A are neutralized by photogenerated electrons of the CB in semiconductor B. When electrons transfer from semiconductor A to semiconductor B, charge carrier separation occurs with a similar mechanism to that of Type II. Meanwhile, the third

generation of Z-scheme photocatalysts was introduced as direct Z-scheme photocatalysts, which are mainly utilized in solar-energy conversion due to their excellent potential for spatial-photogenerated electron–hole pair separation and their optimized oxidation and reduction ability. In fact, a simple Z-scheme photocatalysis is very much like Type-II heterojunction photocatalysis, but it has a distinct charge-carrier migration mechanism [58], as presented in Figure 16.

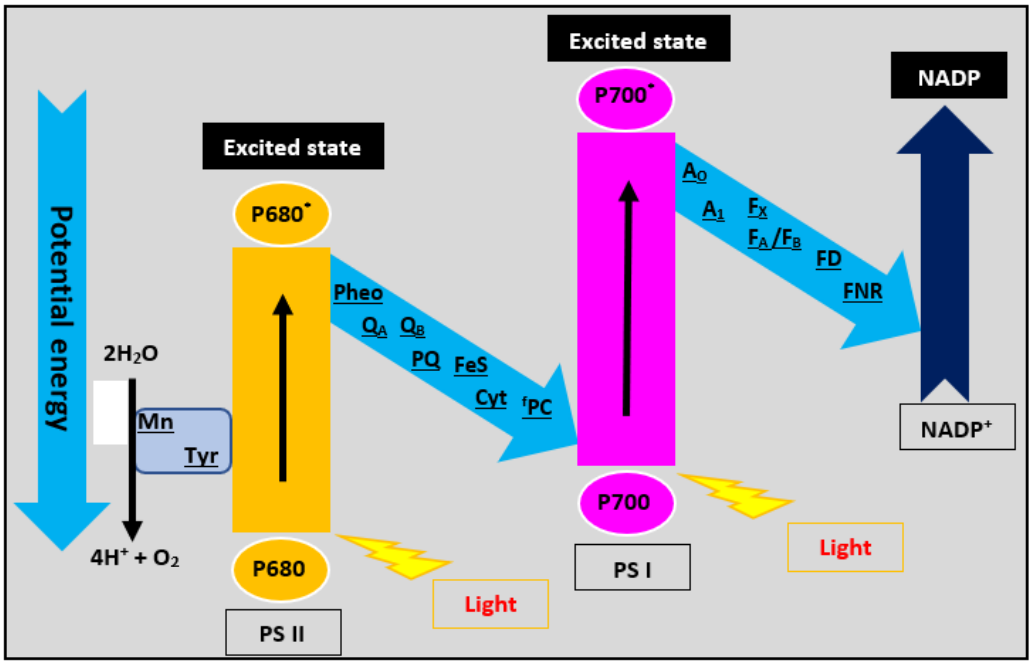

Figure 15. Schematic representation of the charge separation mechanism in natural photosynthesis known as the Z-scheme.

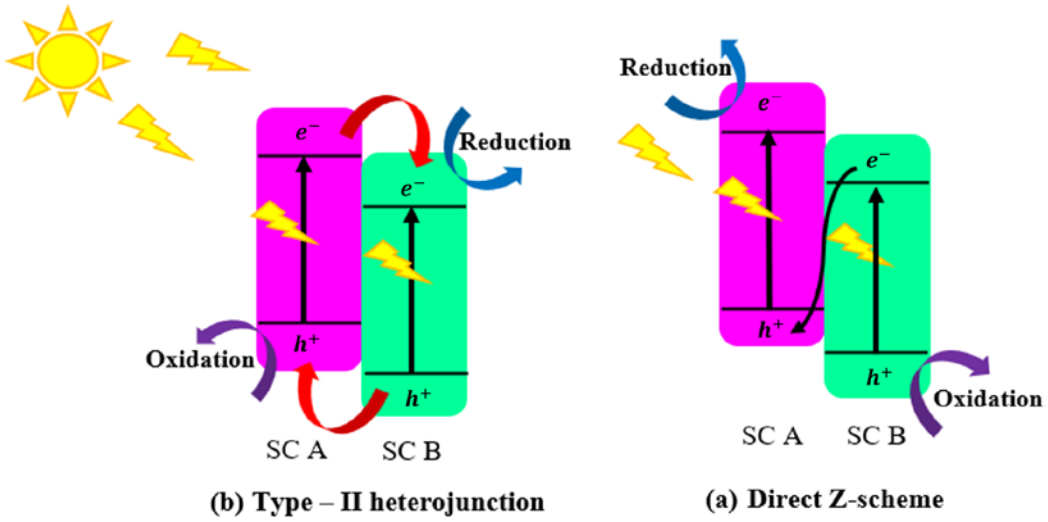

Figure 16. The schematic illustration and the correlation between the mechanism of charge-carrier separation in (**a**) Type-II heterojunction and (**b**) the direct Z-scheme.

The majority of the semiconductors with the Z-scheme mechanism have been produced from g-C_3N_4 and are most studied and investigated in hydrogen production and dye degradations [59–61]. Water splitting by Z-scheme was first introduced by Bard et al. [62] in 1979; since then, it has been rapidly developed and utilized. In Z-scheme water splitting, reversible redox mediators such as Fe^{3+}/Fe^{2+}, IO^{3-}/I^{-}, and NO^{3-}/NO^{2-} are commonly

utilized as electron transport chains [57]. The utilization of the Z-scheme mechanism has some advantages compared to single-component photocatalysts and heterojunction-type nanocomposites, including small bandgap, further suppression of electron–hole pairs' recombination, and favorable band-edge position with substantially large overpotential. The efficient charge separation and enhanced activity were reported in the Z-scheme-based semiconductor systems with various morphologies and catalysts, such as WO_3-g-C_3N_4 [63], MoO_3-g-C_3N_4 [60], Bi_2O_3-$NaNbO_3$ [64], $BiVO_4$-g-C_3N_4 [65], and AgI-Bi_2O_3 [66]. It was reported that glyphosate, which is commonly used in herbicidal applications, is a toxic and cancerogenic material and must be degraded; one of the best options for this is semiconductor photocatalysts for the treatment of organic pollutants. In this regard, visible-light-active photocatalysts are of special interest; bismuth tungstate (Bi_2WO_6), having visible-light absorption (Eg ≈ 2.7 eV), satisfactorily stability, low toxicity, and very potent oxidation capability toward organic contamination, seems to be a promising candidate for glyphosate degradation [67].

In comparison with the pure hierarchical Bi_2WO_6 and WO_3/Bi_2WO_6, the $Ag/WO_3/Bi_2WO_6$ heterojunction presents improved photocatalytic behavior in the removal of gaseous chlorobenzene under simulated sunlight. It was reported that 2% $Ag/WO_3/Bi_2WO_6$ heterojunction has up to 2.5- and 1.9-times higher conversion efficiency than that of the pristine Bi_2WO_6 and WO_3/Bi_2WO_6 samples. This upgraded photocatalytic activity can be related to the fabrication of three-component heterojunction and SPR of Ag NPs, which can not only improve the visible-light absorption, but also enhance the separation efficiency of the photogenerated electrons and holes in the hybrids.

One of the effective strategies to promote Bi_2WO_6 performance is to combine it with other semiconductors through the Z-scheme mechanism. Accordingly, Tang et al. [68] synthesized a hierarchical Cu_2S/Bi_2WO_6 heterojunction through a three-step route by the Z-scheme mechanism, as shown in Figure 17, to enhance the photocatalytic performance of glyphosate degradation under irradiation of visible light. This Cu_2S/Bi_2WO_6 heterojunction exhibited an improved visible-light photocatalytic performance and led to far better results than just Bi_2WO_6 or Cu_2S. This enhanced performance was related to hierarchical morphology, considerable absorption of visible light, and utilization of the Z-scheme mechanism [68].

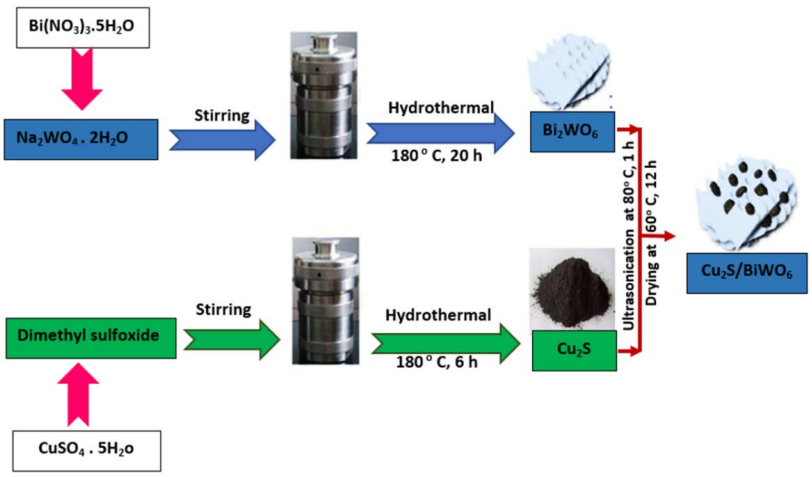

Figure 17. Schematic illustration of production route of hierarchical Cu_2S/Bi_2WO_6 photocatalysts.

The binary $Bi_2WO_6/CuBi_2O_4$ heterojunction photocatalytic hybrid to degrade ciprofloxacin was synthesized through a one-step Z-scheme mechanochemical operation with a solid-state system [69]. This Z-scheme-based heterojunction presented an excellent photocatalytic activity in the ciprofloxacin degradation under simulated sunlight ($\lambda > 420$ nm). This hybrid $Bi_2WO_6/CuBi_2O_4$ heterojunction demonstrated an improved separation and migration efficiency toward photogenerated charge carriers due to its p-n heterojunction condition

and the corresponding high redox capability. The investigation of the related mechanism exhibited that the charge transfer path follows the Z-scheme model with the crucial role of H^+ and $^{\bullet}O^{2-}$. In this regard, during the mechanochemical synthesis process of the $Bi_2WO_6/CuBi_2O_4$ heterojunction, 2 g of Bi_2O_3 was ground with WO_3 or CuO at a specific molar ratio. Subsequently, the produced $Bi_2WO_6/CuBi_2O_4$ hybrids were further processed by grinding a 2 g mixture of Bi_2O_3, CuO, and WO_3 with $Bi_2WO_6/CuBi_2O_4$ molar ratios of about 10%, 20%, and 30%. The one-step mechanochemical Z-scheme-based $Bi_2WO_6/CuBi_2O_4$ heterojunction production process has substantial potential to achieve efficient CIP decomposition.

In another recent study, Li et al. [70] produced a 2D/2D g-C_3N_4/Au/Bi_2WO_6 heterojunction based on a Z-scheme photocatalyst with improved photocatalytic activity. This visible-light-driven photocatalyst was generated through photoreduction and hydrothermal reaction methods. The excellent photocatalytic activity was related to 2D/2D Z-scheme architecture, which supplied a large number of active sites and efficiently enhanced the separation of photogenerated carriers. In this type of 2D/2D g-C_3N_4/Au/Bi_2WO_6 heterojunction, the Au nanoparticles acted as the redox mediator between g-C_3N_4 and Bi_2WO_6 to improve the transmission and separation of photogenerated electron–hole pairs [70].

2.4.4. Type IV: Heterojunctions with S-Scheme Mechanism

Despite the numerous advantages of traditional heterojunction systems and the Z-scheme group, they suffer from various shortcomings, which will be solved. Accordingly, a new group of heterojunction mechanisms was introduced for semiconductors, known as the S-scheme mechanism. The S-scheme heterojunction has both types of photocatalyst, oxidation photocatalysts (OP) and reduction photocatalysts (RP), with staggered band structures and similarities to the Type II heterojunction. However, the S-scheme mechanism has a very different charge-transfer condition; Figure 18 schematically shows the difference between Type II and S-scheme heterojunction. It should be noted that RPs have high CB and are commonly used in solar fuels. In RPs, electrons should be eliminated by sacrificial agents since they are more effective than photogenerated holes, although OPs are commonly used in environmental degradation, and in this case, holes are the main contributive factors and electrons are useless [71]. According to Figure 18, the typical Type II heterojunction has poor redox ability since electrons and holes are respectively piled up on the CB of OP and VB of RP. In contrast, in an S-scheme heterojunction, the energetic electrons and holes are respectively accumulated in the CB of RP and VB of OP, and the useless photogenerated charge carriers are recombined and lead to a powerful redox potential [72–74]. Hence, the S-scheme charge-transfer route follows the "step" shape at the macroscopic level (from low CB to high CB, Figure 18b), resembling the letter S, while microscopically resembling the letter N.

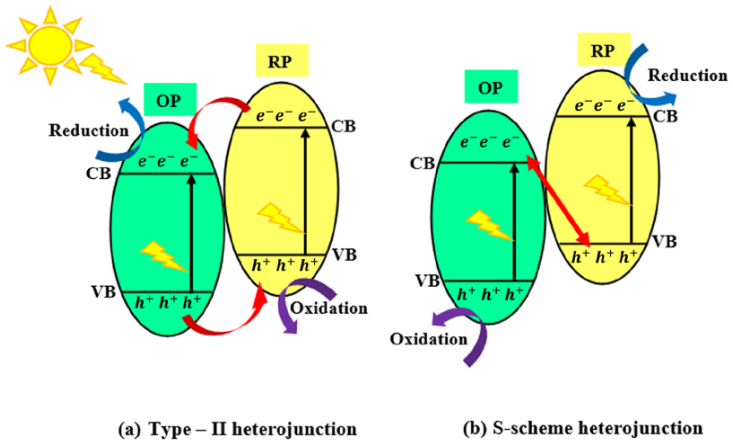

Figure 18. Schematic illustration of (**a**) Type II heterojunction and (**b**) S-scheme heterojunction.

The S-configuration for the heterojunction allows for increased efficiency through high internal electric fields, bending of bands, and increased Coulomb attraction. These increase the driving force, allowing for the recombination of electrons in the CB of OP and hole rearrangement in the VB of RP. Therefore, the unproductive electrons and holes are successfully excluded through recombination, and the productive electrons and holes are retained to be enrolled in photocatalytic reactions. Figure 19 shows the development of these three main factors: **(a)** As seen in Figure 19a, RP has higher CB and VB band positions and lower work function than OP; when these two semiconductors are close to each other (before contact), the electrons of RP transfer to OP, thus creating an electron depletion and electron accumulation layer adjacent to the interface. Concurrently, the negatively charged OP and positively charged RP produce an internal electric field directed from RP to OP; Figure 19b. This produced electric field effectively accelerates the transfer of photogenerated electrons from OP to RP. **(b)** When OP and RP are connected, their relative Fermi levels should also be aligned, inducing an upward and downward shift in the Fermi levels of OP and RP. In this regard, the band bending forced the accumulated photogenerated species at the interface region (electrons in the CB of OP and holes in the VB of RP) to be recombined. **(c)** Due to Coulombic attraction between holes and electrons, holes in the VB of RP and electrons in the CB of OP are tilted and inclined to recombine at the interface [75–77]. It should be noted that S-scheme photocatalysts have numerous applications in different fields such as hydrogen production [78–80], disinfection against bacteria [81,82], and pollutant degradation [83,84]. The S-scheme charge transfer mechanism of TiO_2 and PDA, before, after, and under irradiation during CO_2 reduction is shown in Figure 20 [77,78]. The effect of potential discontinuity in bands, and the overlapping of bands in three different heterojunctions, is shown in Figure 21. As shown, charge carriers' movement between the band levels of Type II heterojunctions maintains the specific charge separation. According to the number of connected semiconductors, heterojunctions can be classified into binary, ternary, and quaternary heterojunctions [79].

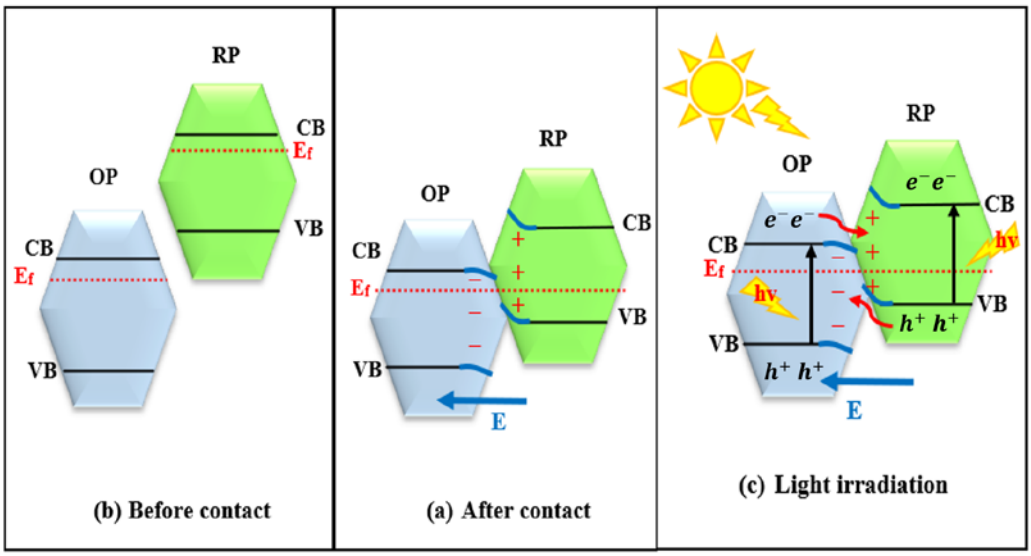

Figure 19. The charge-transfer processes leading to enhanced efficiency in an S-scheme heterojunction, before contact (**b**), after contact (**a**) and with light irradiation (**c**).

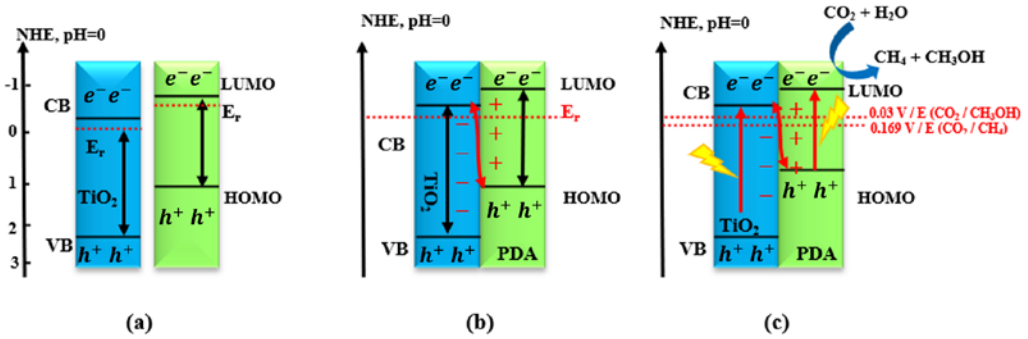

Figure 20. Schematic illustration of the relative band energy positions of TiO_2 and PDA before contact (**a**), after contact (**b**), and under irradiation (**c**), and the S-scheme charge transfer mechanism between TiO_2 and PDA under irradiation.

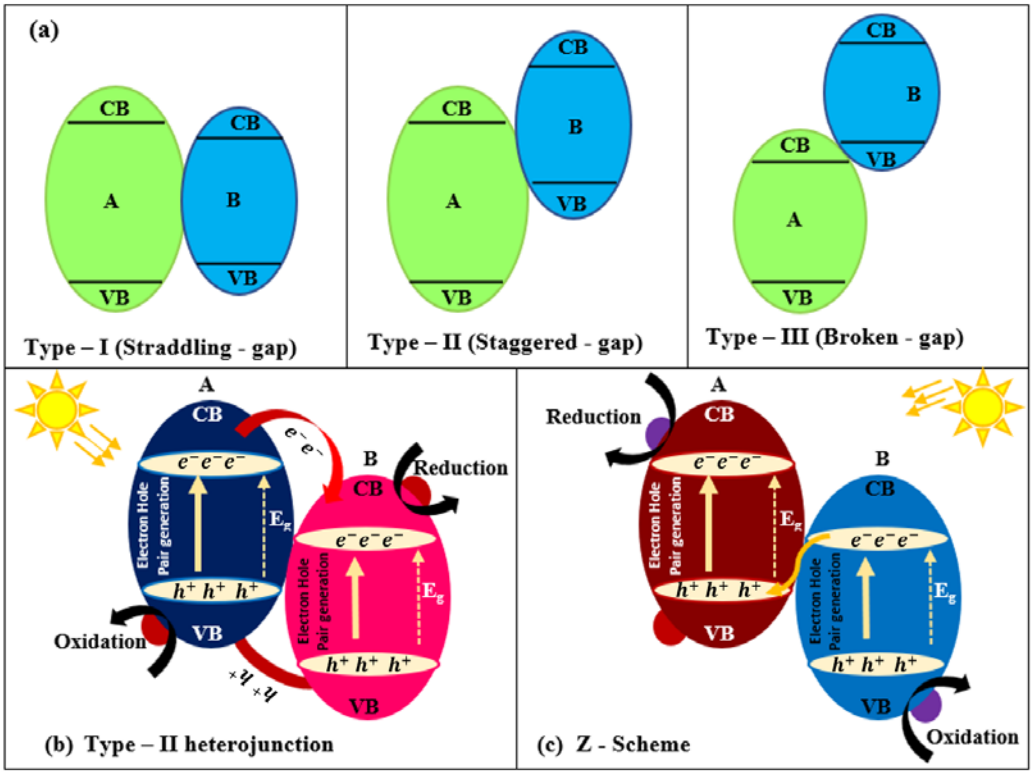

Figure 21. (**a**) Schematic illustration of three types of heterojunction. Charge generation and movement in (**b**) Type II heterojunction and (**c**) Z-scheme heterojunction.

The S-scheme photocatalysts can help to overcome the low solar-to-hydrogen (STH) conversion efficiency, leading to further improved water splitting and hydrogen production. Moreover, the S-scheme heterojunction has considerable superiority in spatial charge separation. The efficiency of the utilization of the S-scheme mechanism in organic pollutant removal, including of pesticides, azo dyes, polyaromatic hydrocarbons, pharmaceutical active, and compounds, is clear and well documented [80]. In addition, S-scheme photocatalysts have great potential to improve solar-to-chemical conversion in hydrogen production. The incineration of fossil fuels induces an unavoidable increment in the CO_2 magnitude of the atmosphere that should effectively be reduced. Due to the challenging process of CO_2 reduction, which has a large thermodynamic barrier and requires multiple reaction steps, photocatalysts utilized in CO_2 reduction should have a potent redox ability to afford the required driving force. In this regard, S-scheme photocatalysts with unique charge-transfer mode are the best candidates for CO_2 reduction and disinfection applications, since pho-

tocatalysts with high redox abilities can substantially disinfect bacteria. In addition, the pollutant degradation efficiency in photocatalysts strongly relies on the productivity of active species with strong oxidation ability, which can be successfully provided by S-scheme heterojunctions.

In a recent study by Fu et al. [81], a novel S-scheme heterojunction concept was proposed in which a two-dimensional (2D)/2D surface-to-surface heterojunction was designed to enhance the activity of photocatalysts. In fact, a greater interfacial contact area enhanced the transfer/separation of interfacial charge carriers. For this aim, Fu et al. [81] fabricated an ultrathin 2D/2D WO_3/g-C_3N_4 step-like composite heterojunction photocatalysts through electrostatic self-assembly of ultrathin tungsten trioxide (WO_3) and graphitic carbon nitride (g-C_3N_4) nanosheets. It was reported that this ultrathin layered heterojunction structure has an excellent capability to promote the surface photocatalytic rate since photogenerated holes and electrons at the heterogeneous interface can readily transfer to the surface of photocatalysts, exhibiting superior H_2-production activity than pure g-C_3N_4 and WO_3.

Recently, it was shown that the CuO/ZnO-based S-scheme heterojunction photocatalysts with mesoporous structures can be utilized to reduce and remove mercury ions [82]. This novel photocatalyst structure was achieved by a wet chemical process in the presence of the F127 surfactant. The synthesized mesoporous CuO/ZnO heterojunctions presented an efficient reduction and removal of Mercury (Hg (II)) ions via visible light. The optimized 3%CuO/ZnO heterojunction exhibited a substantial photoreduction/removal efficiency toward Hg(II), reaching up to 100% within 60 min; this value is about 14 to 24 times higher than those of P-25 and pristine ZnO NPs [82]. This substantial photoreduction/removal efficiency is related to the mesoporous structure, promoting the light utilization rate due to its special architecture, incrementing the surface area and pore volume, enhancing mass diffusion, supplying more active sites, and raising photoinduced electrons [82]. During the S-scheme heterojunction photocatalytic mechanism in the reduction and removal of Mercury (Hg (II)) ions via visible light by mesoporous CuO/ZnO heterojunctions, the CB edge of Cu (~4.96 eV) is more negative than ZnO (~4.19); thus, when the heterojunction is exposed to visible light, the VB of CuO is stimulated to its CB, reducing the adsorbed O_2 on the CuO surface to the $O_2^{-\bullet}$ radical. Then, the adsorbed Hg (II) is reduced by the $O_2^{-\bullet}$ radical onto the CB of CuO. Moreover, the photoinduced electrons shifted from CB of ZnO to VB holes in ZnO to generate $^{\bullet}$OH radicals. Subsequently, the adsorbed HCOOH scavenges holes oxidized through $^{\bullet}$OH radicals onto ZnO's VB for conducting photocatalytic oxidation. Hence, the significant improvement in photocatalytic efficiency of ZnO/CuO heterojunction is related to effective photoinduced carrier separation and the favorable adjustment of band edges, based on the S-scheme mechanism [71].

Jin et al. [83] fabricated graphdiyne (GD)-based heterojunction composite through S-scheme for effective photocatalytic hydrogen production by novel CuIGD/g-C_3N_4 composite. This CuI-GD/g-C_3N_4 nanocomposite was produced through a simple calcination process and, because of the inhibited recombination of photoinduced electron–hole pairs, the photocatalytic activity and performance were considerably improved and led to a high hydrogen evolution rate [83]. It was proved that the chemical integration phenomenon that occurred by GD between g-C_3N_4 and CuI had a great impact on improving electron transfer and facilitating the interface charge transfer trend [83].

In another investigation, Xia et al. [84] constructed a 0D/2D S-scheme-based heterojunction encompassing CeO_2 quantum dots along with polymeric carbon nitride (CeO_2/PCN) via in situ wet chemistry followed by heat treatment. This novel heterojunction demonstrated a high-efficiency photocatalytic sterilization rate of about ~88% towards bacterial *Staphylococcus Aureus* (*S. aureus*) under visible-light irradiation, which was 2.7 and 8.2 times higher than that of pure CeO2 and PCN [84]. This enhanced photocatalytic antibacterial performance is due to the resultant redox proficiency, and the efficient capability of CeO_2/PCN heterojunction in the separation and transfer process of photogenerated charge carriers [84]. Recently, the S-scheme-based WO_3/TiO_2 heterojunction produced by a facile

one-step hydrothermal method showed an improved photocatalytic H_2-fabrication activity via graphene modification [85].

In this ternary heterojunction composite, and in order to produce a novel S-scheme heterojunction, TiO_2 and WO_3 nanoparticles closely stick to reduced graphene oxide (rGO). In this composite, rGO, acting as an ideal support, provides numerous adsorptions and catalytically active sites, and enhances electron separation and transformation through the conduction band of TiO_2 (by supplying a Schottky junction between TiO_2 and rGO), leading to suppressed recombination of electron–hole pairs [85]. Moreover, Deng et al. [86] fabricated a p-type $ZnMn_2O_4$ and n-type ZnO heterojunction based on an S-scheme mechanism in order to promote CO_2 reduction performance since it is beneficial to evolve CO_2 into energy-dense hydrocarbon fuels through photocatalytic CO_2 reduction. For this aim, hierarchical $ZnMn_2O_4$/ZnO nanofibers were synthesized as photocatalysts via electrospinning and calcination processes. This novel design led to the generation of more active sites with multiple light reflections, and enhanced interface charge transfer [86].

In addition to the used heterojunction scheme and the structure of photocatalysts, numerous factors can affect the hydrogen production efficiency, including the active layer morphology, microstructure, and molecular weight [87,88]; ultimately, however, what matters most is the hydrogen production rate, reduction efficiency, and quantum yield. Table 1 briefly lists some of the investigations conducted into the heterojunction semiconductors along with their resultant efficiency in hydrogen evolution.

Table 1. Some investigations into heterojunction semiconductors with their hydrogen production rate.

Semiconductor	Materials Involved in Heterojunction	Application/Result	Hydrogen Production Rate (μmol h^{-1} g^{-1})	Ref
TiO_2-based	Carbon coated Ni/TiO_2	Photostability in an aqueous suspension	2000	[89]
	graphene/TiO_2	H_2-production activity in aqueous solutions containing methanol	736	[90]
	In_2S_3/(Pt-TiO_2)	Photocatalytic H_2 production	1350	[91]
	Au/TiO_2	Excellent photoelectrochemical response	0.5	[92]
	V_2O_5/N,S–TiO_2	Improved H_2 production and phenol degradation	2966	[93]
	TiO_2/$AgGaS_2$	Improved H_2 production rate	4200	[94]
	Fe_2O_3/TiO_2	Improved H_2 production rate	7253	[95]
	Pt@TiO_2@In_2O_3@MnO_x	High photocatalytic activity toward water and alcohol oxidation.	-	[10]
	WO_3/TiO_2 with graphene modification	Promoted photocatalytic H_2 production activity	245.8	[85]
	Macro−Mesoporous TiO_2−Graphene	Enhanced capacity for rapid adsorption and photodegradation of organic dyes	-	[11]
	Au/TiO_2	Light intensity plays a key role in photocatalysis	7–9 kW/m^2	[12]
	TiO_2/C_3N_4/Ti_3C_2	Improved CO_2 reduction activity	CO yield: 3.14	[77]
	TiO_2/polydopamine	Improved CO_2 reduction activity and selectivity	Methane yield: 1.50	[78]
CdS-based	CdS nanorods/CdSe	Improved H_2 production rate	40,500	[96]
	CeO_2/CdS	Promoted photocatalytic hydrogen activity	223	[97]
	CdS/ZnS/In_2S_3	Promoted photocatalytic hydrogen activity	8100	[98]
	MoS_2/G-CdS	Improved H_2 production rate	9000	[99]
	CdS nanorods/Cu_2MoS_4	Superior photocatalytic activity for H_2 evolution	15,560	[6]
	CdS-based MOFs	Without co-catalyst material for highly efficient photocatalytic H_2 evolution	26,100	[54]
	$SnNb_2O_6$/CdS-diethylenetriamine	Excellent photocatalytic hydrogen production.	7808	[100]

Table 1. *Cont.*

Semiconductor	Materials Involved in Heterojunction	Application/Result	Hydrogen Production Rate ($\mu mol\ h^{-1}\ g^{-1}$)	Ref
Graphitic carbon nitride-based	g-C_3N_4/zinc phthalocyanine	Sensitizer of Graphitic Carbon Nitride	12,500	[101]
	WO_3/g-C_3N_4	Enhanced photocatalytic activity	110	[63]
	$ZnFe_2O_4$/g-C_3N_4	Efficient solar H_2 generation	200.77	[102]
	g-C_3N_4–$SrTiO_3$:Rh	Enhanced H_2 evolution	2223	[103]
	(g-C_3N_4)–Pt-TiO_2	Photocatalytic H_2 production	1780	[104]
	K–I co-doped g-C_3N_4	Enhanced charge separation efficiency	41.23	[9]
	g-C_3N_4/Au/Bi_2WO_6	Promoted visible-light-driven photocatalytic activity	-	[70]
	WO_3/g-C_3N_4	Excellent photocatalytic H_2 generation activity	982	[81]
	g-C_3N_4/WO_3/AgI	Enhanced performance for neonicotinoid degradation	-	[28]
	SnS2/RGO/g-C_3N_4	Enhanced photocatalytic activity for H_2 generation	2050	[25]
	CuI-GD/g-C_3N_4	Efficient photocatalytic H_2 evolution	43	[83]
	g-C_3N_4–TiO_2	Photocatalytic degradation of formaldehyde in air	-	[61]
	WO_3/g-C_3N_4	Enhanced photocatalytic activity with high dependency to WO_3 content	110	[63]
CdS and TiO_2 -based	sub-nanometer thick layered TiO_2 nanosheet/CdS (QDs)	Efficient solar H_2 generation	1000	[105]
	Chromosilicate decorated with (CdS/C or CdS-TiO_2/C)	Improved H_2 production rate	2580	[106]
	Au@TiO_2–CdS	Efficient solar H_2 generation	1970	[107]
Other	$KTaO_3$	Reduction in band gap leading to enhanced absorption of visible light	-	[8]
	N-doped graphene ((N)G)	High efficiency for the photocatalytic generation of H2 from water/methanol mixtures	336–4999	[13]
	ZnO@ZnS micro/nanoferns	Excellent photocatalytic performance to decontaminate inorganic-organic biopollutant systems	-	[16]
	Calcium silicate hydrate (CSH) nanosheets	Harmful heavy metals in polluted water are removed and collected by adsorbents	CO yield: 17,100	[20]
	BiVO4/Ti_3C_2 nanosheets	Improved photocatalytic activity	Up to 1800	[27]
	Ag/$LaVO_4$/$BiVO_4$	Enhanced photocatalytic H_2 evolution	3720	[33]
	AgI-decorated β-Bi_2O_3	Efficient degradation of organic pollutants	-	[66]
	Ag/ZnO nanosheets	Enhanced visible-light degradation	443.6	[44]
	$ZnIn_2S_4$ microflowers	Improved kinetics process of charge-carriers for photocatalytic H2 evolution	2400	[47]
	ZnO/$ZnBi_2O_4$	Durable visible-light-activated photocatalysts for efficient removal of organic pollutants	-	[50]
	$ZnBi_2O4$/ZnO	Enhanced H_2 production and BPA degradation	3440	[108]
	$BiIO_4$/$BiVO_4$	Promoted visible-light-induced photocatalytic performance for rhodamine B degradation and photocurrent evolution	-	[53]
	Bi_2O_3/$NaNbO_3$	Highly active photocatalytic performance	-	[64]

2.5. Multi-Component, Hybrid, and Other Semiconductor Heterojunctions

Because of several limitations in two-component heterojunction photocatalysts, such as lower region of visible-light response, multi-component heterojunction systems are introduced with an electron transfer system and some visible-light active components (two or more) that are spatially accommodated. Mostly, multi-component heterojunctions consist of two semiconductors and one metal [45]. Figure 22 shows the schematic of a typical multi-component heterojunction system where two semiconductors of A and B (S-A and S-B) can be stimulated by UV/visible light with various photo-absorption ranges; the juxtaposition of their photo-absorption can significantly expand the UV/visible-light photo-response range. The first photocatalytic action is the adsorption of photons from the UV and from

the visible light. Photons have energies that are equal to or higher than the bandgap of S-A and S-B, producing holes in VB and electrons in CB. Then, electrons in the CB of S-A are allowed to flow into the metal by the Schottky barrier (electron transfer I: S-A → metal) since the CB of S-A is higher with respect to the metal. The I electron transfer process is faster than the electron–hole recombination among VB and CB of S-A. For this reason, many electrons (in CB of S-A) can accumulate into the metal. This results in the production of many holes with consequent oxidation in the VB of S-A. This provides excellent results because an increased number of holes allows increased oxidation of the pollutants or OH^-. By comparison, holes in the VB of S-B can easily flow into the metal due to the increased energy magnitude of the metal with respect to the VB of S-B. This takes place through the mechanism of electron transfer II: metal → S-B, which acts more quickly with respect to the electron–hole recombination among the VB and CB of S-B. In this way, an increased number of electrons are available to reduce all the absorbed compounds such as H^+ and O_2. As a consequence, an increased number of electrons can transfer due to the stimulation of S-A and S-B through light. Thus, in the described electron transfer process, the employed metal allows for the storing or for the activation of sites for the electrons' recombination in the CB of S-A and for the recombination of holes in the VB of S-B. This is due to the increase in the interfacial charge transfer and to the improvement in the full separation of holes in the VB of S-A and electrons in the CB of S-B [45]. As a general consideration, the multi-component heterojunction system allows for increased photocatalytic activity with respect to configurations with a single semiconductor or semiconductor heterojunctions.

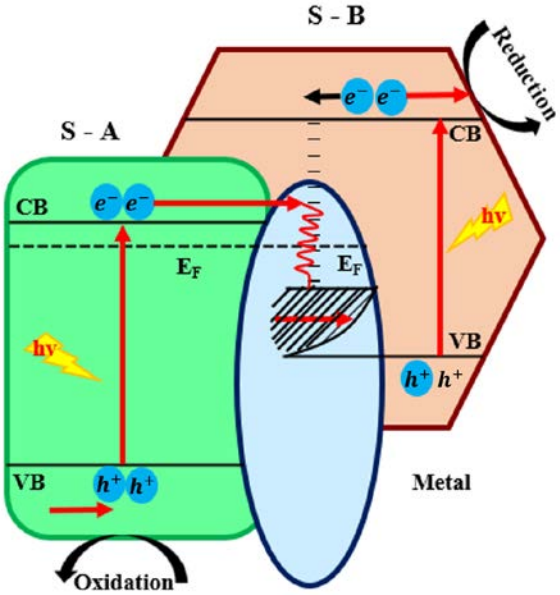

Figure 22. Schematic illustration of a typical multi-component heterojunction system.

In addition to the mentioned methods, some high-efficiency heterojunction photocatalysts can be produced through novel methods, namely, ultrasound-assisted synthesis schemes. Lin et al. [109] developed high throughput Ag_3PO_4/CeO_2 heterojunction photocatalysts using an ultrasound-assisted method with significantly improved photocatalytic activity in comparison to pure Ag_3PO_4, CeO_2, and Ag_3PO_4/CeO_2 ones without ultrasound application. The improved activity in the photocatalysis process is related to the shapely and appropriate construction of the Ag_3PO_4/CeO_2 heterostructure.

Recently, hybrid photocatalysts have attracted much attention. Tho et al. [110] proposed a novel efficient $rGO/ZnBi_2O_4$ hybrid catalyst generated through oxidation-reduction and coprecipitation techniques. It seems that $rGO/ZnBi_2O_4$ is a favorable, economic, and promising green photocatalyst candidate for environmental remediation applications, and its advantageous performance is related to rGO (reduced graphene oxide).

It was shown that the rGO/$ZnBi_2O_4$ in a suitable aqueous solution and under visible-light irradiation can effectively degrade the toxic organic pollutant 2,4-D. The rGO species serve as superior e^- acceptors and mediators, improving the photoinduced e^- transfer and preventing the recombination of photoinduced e^-/H^+ pairs.

The novel $CeO_2/PbWO_4$ nanocomposite heterojunction semiconductor photocatalysts that were activated by UV and/or visible-light irradiation were fabricated via a simplistic hydrothermal method to effectively photodegrade the Methylene Blue (MB) dye [111]. This $CeO_2/PbWO_4$ heterojunction demonstrated the significant photodegradation efficacy of about 94% toward MB aqueous dye during 140 min of irradiation in visible light, which is considerably higher than that of traditional ones. This $CeO_2/PbWO_4$ heterojunction possesses excellent charge separation/transfer, decreased bandgap, and powerful visible-light absorption since it inhibits the photoexcited charge recombination [111].

Hybrid nanoparticles can assemble onto the halloysite support via microwave-assisted methods to enhance photocatalytic performance. In this regard, halloysite-CeO_2-AgBr nanocomposites were generated through a facile microwave-assisted process with a great impact of molar fractions on photocatalytic activity [112]. It was shown that both the high adsorptive potential of halloysite and improved electron transfer in CeO_2-AgBr effectively assisted the photocatalytic methyl orange degradation [112].

3. Conclusions and Future Prospective

The presented review paper aimed to introduce and discuss the semiconductor-based routes to fabricate novel photocatalysts stimulated by visible-light irradiation in order to generate green and renewable solar fuels such as H_2. Hydrogen is considered to be one of the most advantageous sustainable energy carriers with great potential to substitute for fossil fuels because of its substantial gravimetric energy density. In addition, it is very clean and its combustion, fortunately, is CO_2 free and leads to water production. In this regard, semiconductor-based photocatalysis procedures have been proven to be a promising scheme in hydrogen production. The catalysis process can be performed using homogeneous and heterogeneous procedures, but the heterogeneous processes are preferred. In semiconductor-based photocatalysis, the photon energy is utilized to generate an electron–hole pair, leading to redox reactions. One of the main issues in achieving enhanced quantum efficiency in photocatalysis procedures is the recombination of photoinduced species. Until now, various strategies have been proposed and explored to overcome the high recombination rate issue; hence, reducing the recombination rate is crucial to allow the photogenerated electron–hole to migrate to the surface and carry out reduction and oxidation reactions with high efficiency. In this regard, the main goal of this review paper is to discuss the design, synthesis, and characteristics of the novel high throughput, visible-light-driven, heterojunction composite photocatalysts for environmental remediation applications. It was seen that many variables are involved in the achievement of these targets, such as crystal structure, morphology, size, composition, element oxidation states, optical absorption properties, electrochemical properties of the proposed heterojunction photocatalysts, photocatalytic mechanism, catalyst dosage, temperature, and initial pH. Therefore, it is of eminent importance to thoroughly understand and wisely tailor the produced semiconductor for the desired application. This important issue requires accurate knowledge of the possible advantages and disadvantages, challenges, and benefits of each parameter and mechanism. It must be noted that the introduction of heterojunction materials has a substantial impact on the improvement in conversion efficiency; for instance, just a slight amount of Ag/WO_3/Bi_2WO_6 heterojunction can improve the conversion rate by up to 250% compared to pristine counterparts. This up-graded activity can be related to the generation of a three-component heterojunction that improves visible-light absorption and increases the separation efficiency of the photogenerated electrons and holes [67]. Moreover, 3% of CuO/ZnO heterojunction can lead to considerable photoreduction with substantial removal efficiency toward Hg(II), reaching 100%, which is 24 times higher than that of pristine ZnO [82].

Semiconductors that have been introduced and used to date, such as two-component heterojunction photocatalysts, have numerous limitations, including the limited region of visible-light response, recombination issues, and unsatisfactory efficiency. Hence, multi-component heterojunction systems are recommended with more visible-light active components. Moreover, novel electron-transfer systems have been proposed that are spatially accommodated. Multi-component heterojunctions consisting of two semiconductors and one metal are among these novel generations. Additionally, hybrid heterojunctions have been designed with the utilization of various nanostructure morphologies. Moreover, additive manufacturing technologies, hierarchical designs, coatings, doping, etc., can considerably help the semiconductor industry to gain the potential to manufacture complex structures and morphologies in order to boost hydrogen production performance [113–118]. Recently, plasmonic nanomaterials have been introduced as frequency-tunable substances with exceptional localized surface plasmon resonance (LSPR) [119,120]. The LSPR stimulation can concentrate and intensify the light energy, and significantly improve the regional electric field at the surface of the nanomaterial and promote the photocatalytic kinetics reaction rate; this strategy was used by Jiang et al. [121] for photocatalytic CO_2 reduction using the $Au/TiO_2/W_{18}O_{49}$ plasmonic heterostructure.

Despite significant progress in the field of heterojunction photocatalysts, considerable issues still remain in the progression of easy, profitable, and economic technologies to generate modern and high throughput heterojunction photocatalysts at the industrial scale for functional applications. Additionally, future designs should accurately control the structure, porosity and surface condition, morphology, contact interface, hierarchical assembly, and crystallinity of substances to attain high quality and efficient heterojunction photocatalysts. Moreover, the literature lacks comprehensive theoretical approaches and modeling investigations; hence, researchers should also work on these subjects. Furthermore, photocatalyst materials, including their design, doping, coating, combination state, dye sensitization, and nanostructuring, and the production of novel materials such as metamaterials with heterostructures, should be considered in future studies. The intelligent designs and steps toward the production of smart materials can also be thought-provoking topics for upcoming research plans.

Author Contributions: Conceptualization, A.B. and B.S.; methodology, A.B.; Software, B.S.; validation, Q.L. and S.R., formal analysis, M.M.D.C.; investigation, Q.L., B.S. and P.D.C.; resources, Q.L. and S.R.; data curation, A.B., B.S. and P.D.C.; writing—original draft preparation, A.B., B.S. and M.M.D.C.; writing—review and editing, Q.L., S.R. and P.D.C.; visualization, A.B., P.D.C.; supervision, Q.L., P.D.C.; project administration, S.R. and Q.L.; funding acquisition, Q.L. and B.S. All authors have read and agreed to the published version of the manuscript.

Funding: The authors acknowledge the support by National Natural Science Foundation of China (Nos. 52072241 and 51772187). This work was also performed during the implementation of the project Building-up Centre for advanced materials application of the Slovak Academy of Sciences, ITMS project code 313021T081, supported by Research & Innovation Operational Programme funded by the ERDF.

Informed Consent Statement: Not applicable.

Data Availability Statement: Not applicable.

Acknowledgments: The authors wish to thank Catalin Pruncu for his insightful and constructive comments and suggestions. They also want to thank the editor and anonymous referees for their careful reading, comments and suggestions which helped to improve the paper.

Conflicts of Interest: The authors declare no conflict of interest.

References

1. Victoria, M.; Haegel, N.; Peters, I.M.; Sinton, R.; Jäger-Waldau, A.; del Cañizo, C.; Breyer, C.; Stocks, M.; Blakers, A.; Kaizuka, I.; et al. Solar photovoltaics is ready to power a sustainable future. *Joule* **2021**, *5*, 1041–1056. [CrossRef]

2. Møller, K.T.; Jensen, T.R.; Akiba, E.; Li, H. Hydrogen—A sustainable energy carrier. *Prog. Nat. Sci. Mater. Int.* **2017**, *27*, 34–40. [CrossRef]
3. Olabi, A.G.; Bahri, A.S.; Abdelghafar, A.A.; Baroutaji, A.; Sayed, E.T.; Alami, A.H.; Rezk, H.; Abdelkareem, M.A. Large-vscale hydrogen production and storage technologies: Current status and future directions. *Int. J. Hydrogen Energy* **2021**, *46*, 23498–23528. [CrossRef]
4. Li, S.; Kang, Q.; Baeyens, J.; Zhang, H.L.; Deng, Y.M. Hydrogen Production: State of Technology. *IOP Conf. Ser. Earth Environ. Sci.* **2020**, *544*, 012011. [CrossRef]
5. Fujishima, A.; Honda, K. Electrochemical Photolysis of Water at a Semiconductor Electrode. *Nature* **1972**, *238*, 37–38. [CrossRef]
6. Hong, S.; Kumar, D.P.; Reddy, D.A.; Choi, J.; Kim, T.K. Excellent photocatalytic hydrogen production over CdS nanorods via using noble metal-free copper molybdenum sulfide (Cu2MoS4) nanosheets as co-catalysts. *Appl. Surf. Sci.* **2017**, *396*, 421–429. [CrossRef]
7. Li, K.; Zhang, S.; Li, Y.; Fan, J.; Lv, K. MXenes as noble-metal-alternative co-catalysts in photocatalysis. *Chin. J. Catal.* **2021**, *42*, 3–14. [CrossRef]
8. Modak, B.; Ghosh, S.K. Improving visible light photocatalytic activity of $KTaO_3$ using cation-anion dopant pair. *Sol. Energy Mater. Sol. Cells* **2017**, *159*, 590–598. [CrossRef]
9. Guo, Y.; Chen, T.; Liu, Q.; Zhang, Z.; Fang, X. Insight into the Enhanced Photocatalytic Activity of Potassium and Iodine Codoped Graphitic Carbon Nitride Photocatalysts. *J. Phys. Chem. C* **2016**, *120*, 25328–25337. [CrossRef]
10. Li, A.; Chang, X.; Huang, Z.; Li, C.; Wei, Y.; Zhang, L.; Wang, T.; Gong, J. Thin Heterojunctions and Spatially Separated Cocatalysts To Simultaneously Reduce Bulk and Surface Recombination in Photocatalysts. *Angew. Chemie Int. Ed.* **2016**, *55*, 13734–13738. [CrossRef]
11. Du, J.; Lai, X.; Yang, N.; Zhai, J.; Kisailus, D.; Su, F.; Wang, D.; Jiang, L. Hierarchically Ordered Macro−Mesoporous TiO_2−Graphene Composite Films: Improved Mass Transfer, Reduced Charge Recombination, and Their Enhanced Photocatalytic Activities. *ACS Nano* **2011**, *5*, 590–596. [CrossRef]
12. Xing, X.; Tang, S.; Hong, H.; Jin, H. Concentrated solar photocatalysis for hydrogen generation from water by titania-containing gold nanoparticles. *Int. J. Hydrogen Energy* **2020**, *45*, 9612–9623. [CrossRef]
13. Lavorato, C.; Primo, A.; Molinari, R.; Garcia, H. N-Doped Graphene Derived from Biomass as a Visible-Light Photocatalyst for Hydrogen Generation from Water/Methanol Mixtures. *Chem. Eur. J.* **2014**, *20*, 187–194. [CrossRef]
14. Molinari, R.; Lavorato, C.; Argurio, P.; Szymański, K.; Darowna, D.; Mozia, S. Overview of Photocatalytic Membrane Reactors in Organic Synthesis, Energy Storage and Environmental Applications. *Catalysts* **2019**, *9*, 239. [CrossRef]
15. Ayodhya, D.; Veerabhadram, G. A review on recent advances in photodegradation of dyes using doped and heterojunction based semiconductor metal sulfide nanostructures for environmental protection. *Mater. Today Energy* **2018**, *9*, 83–113. [CrossRef]
16. Serrà, A.; Gómez, E.; Philippe, L. Bioinspired ZnO-Based Solar Photocatalysts for the Efficient Decontamination of Persistent Organic Pollutants and Hexavalent Chromium in Wastewater. *Catalysts* **2019**, *9*, 974. [CrossRef]
17. Ebrahimi, M.; Shaeri, M.H.; Gode, C.; Armoon, H.; Shamsborhan, M. The synergistic effect of dilute alloying and nanostructuring of copper on the improvement of mechanical and tribological response. *Compos. Part B Eng.* **2019**, *164*, 508–516. [CrossRef]
18. Ebrahimi, M.; Shamsborhan, M. Monotonic and dynamic mechanical properties of PTCAE aluminum. *J. Alloys Compd.* **2017**, *705*, 28–37. [CrossRef]
19. Ichikawa, S.; Doi, R. Hydrogen production from water and conversion of carbon dioxide to useful chemicals by room temperature photoelectrocatalysis. *Catal. Today* **1996**, *27*, 271–277. [CrossRef]
20. Chen, L.; Wang, X.; Chen, Y.; Zhuang, Z.; Chen, F.-F.; Zhu, Y.-J.; Yu, Y. Recycling heavy metals from wastewater for photocatalytic CO_2 reduction. *Chem. Eng. J.* **2020**, *402*, 125922. [CrossRef]
21. Qin, G.; Zhang, Y.; Ke, X.; Tong, X.; Sun, Z.; Liang, M.; Xue, S. Photocatalytic reduction of carbon dioxide to formic acid, formaldehyde, and methanol using dye-sensitized TiO_2 film. *Appl. Catal. B Environ.* **2013**, *129*, 599–605. [CrossRef]
22. Pietro, A.; Cristina, L.; Raffaele, M. Hydrogen Production and Organic Synthesis in Photocatalytic Membrane Reactors: A Review. *Int. J. Membr. Sci. Technol.* **2020**, *7*, 1–14. [CrossRef]
23. Molinari, R.; Lavorato, C.; Argurio, P. Visible-Light Photocatalysts and Their Perspectives for Building Photocatalytic Membrane Reactors for Various Liquid Phase Chemical Conversions. *Catalysts* **2020**, *10*, 1334. [CrossRef]
24. Li, S.; Zhang, H.; Nie, J.; Dewil, R.; Baeyens, J.; Deng, Y. The Direct Reduction of Iron Ore with Hydrogen. *Sustainability* **2021**, *13*, 8866. [CrossRef]
25. Lu, N.; Jing, X.; Zhang, J.; Zhang, P.; Qiao, Q.; Zhang, Z. Photo-assisted self-assembly synthesis of all 2D-layered heterojunction photocatalysts with long-range spatial separation of charge-carriers toward photocatalytic redox reactions. *Chem. Eng. J.* **2022**, *431*, 134001. [CrossRef]
26. Liu, L.; Zhang, Y.; Huang, H. Junction Engineering for Photocatalytic and Photoelectrocatalytic CO_2 Reduction. *Sol. RRL* **2021**, *5*, 2000430. [CrossRef]
27. Li, Y.; Liu, Y.; Xing, D.; Wang, J.; Zheng, L.; Wang, Z.; Wang, P.; Zheng, Z.; Cheng, H.; Dai, Y.; et al. 2D/2D heterostructure of ultrathin $BiVO_4/Ti_3C_2$ nanosheets for photocatalytic overall Water splitting. *Appl. Catal. B Environ.* **2021**, *285*, 119855. [CrossRef]
28. Tang, M.; Ao, Y.; Wang, C.; Wang, P. Rationally constructing of a novel dual Z-scheme composite photocatalyst with significantly enhanced performance for neonicotinoid degradation under visible light irradiation. *Appl. Catal. B Environ.* **2020**, *270*, 118918. [CrossRef]

29. Wang, S.; Han, X.; Zhang, Y.; Tian, N.; Ma, T.; Huang, H. Inside-and-Out Semiconductor Engineering for CO_2 Photoreduction: From Recent Advances to New Trends. *Small Struct.* **2021**, *2*, 2000061. [CrossRef]
30. Djavanroodi, F.; Ebrahimi, M.; Nayfeh, J.F. Tribological and mechanical investigation of multi-directional forged nickel. *Sci. Rep.* **2019**, *9*, 241. [CrossRef]
31. Fajrina, N.; Tahir, M. A critical review in strategies to improve photocatalytic water splitting towards hydrogen production. *Int. J. Hydrogen Energy* **2019**, *44*, 540–577. [CrossRef]
32. Moniz, S.J.A.; Shevlin, S.A.; Martin, D.J.; Guo, Z.-X.; Tang, J. Visible-light driven heterojunction photocatalysts for water splitting—A critical review. *Energy Environ. Sci.* **2015**, *8*, 731–759. [CrossRef]
33. Liu, Z.; Yu, Y.; Zhu, X.; Fang, J.; Xu, W.; Hu, X.; Li, R.; Yao, L.; Qin, J.; Fang, Z. Semiconductor heterojunctions for photocatalytic hydrogen production and Cr(VI) Reduction: A review. *Mater. Res. Bull.* **2022**, *147*, 111636. [CrossRef]
34. Peroulis, D.; Waghmare, P.R.; Mitra, S.K.; Manakasettharn, S.; Taylor, J.A.; Krupenkin, T.N.; Zhu, W.; Nessim, G.D.; Marano, F.; Guadagnini, R.; et al. Conduction Mechanisms in Organic Semiconductors. In *Encyclopedia of Nanotechnology*; Springer: Dordrecht, The Netherlands, 2012; pp. 493–500.
35. Ali, R.H. New Trends for Removal of Water Pollutants. In *Prime Archives in Material Science*; Heimann, R.B., Ed.; Vide Leaf, Hyderabad: Hyderabad, India, 2020.
36. Kisch, H. Semiconductor Photocatalysis-Mechanistic and Synthetic Aspects. *Angew. Chemie Int. Ed.* **2013**, *52*, 812–847. [CrossRef] [PubMed]
37. Wang, W.; Tadé, M.O.; Shao, Z. Research progress of perovskite materials in photocatalysis- and photovoltaics-related energy conversion and environmental treatment. *Chem. Soc. Rev.* **2015**, *44*, 5371–5408. [CrossRef]
38. Böer, K.W. Semiconductor Heterojunctions. In *Survey of Semiconductor Physics*; Springer Netherlands: Dordrecht, The Netherlands, 1992; pp. 676–700.
39. Low, J.; Yu, J.; Jaroniec, M.; Wageh, S.; Al-Ghamdi, A.A. Heterojunction Photocatalysts. *Adv. Mater.* **2017**, *29*, 1601694. [CrossRef]
40. Su, Q.; Li, Y.; Hu, R.; Song, F.; Liu, S.; Guo, C.; Zhu, S.; Liu, W.; Pan, J. Heterojunction Photocatalysts Based on 2D Materials: The Role of Configuration. *Adv. Sustain. Syst.* **2020**, *4*, 2000130. [CrossRef]
41. Zhu, C.; Liu, Y.; Cao, H.; Sun, J.; Xu, Q.; Wang, L. Insight into the influence of morphology of Bi_2WO_6 for photocatalytic degradation of VOCs under visible light. *Colloids Surfaces A Physicochem. Eng. Asp.* **2019**, *568*, 327–333. [CrossRef]
42. Li, X.; Huang, R.; Hu, Y.; Chen, Y.; Liu, W.; Yuan, R.; Li, Z. A Templated Method to Bi_2WO_6 Hollow Microspheres and Their Conversion to Double-Shell Bi_2O_3/Bi_2WO_6 Hollow Microspheres with Improved Photocatalytic Performance. *Inorg. Chem.* **2012**, *51*, 6245–6250. [CrossRef]
43. Farhadian, M.; Sangpour, P.; Hosseinzadeh, G. Morphology dependent photocatalytic activity of WO_3 nanostructures. *J. Energy Chem.* **2015**, *24*, 171–177. [CrossRef]
44. Mou, H.; Song, C.; Zhou, Y.; Zhang, B.; Wang, D. Design and synthesis of porous Ag/ZnO nanosheets assemblies as super photocatalysts for enhanced visible-light degradation of 4-nitrophenol and hydrogen evolution. *Appl. Catal. B Environ.* **2018**, *221*, 565–573. [CrossRef]
45. Wang, H.; Zhang, L.; Chen, Z.; Hu, J.; Li, S.; Wang, Z.; Liu, J.; Wang, X. Semiconductor heterojunction photocatalysts: Design, construction, and photocatalytic performances. *Chem. Soc. Rev.* **2014**, *43*, 5234. [CrossRef] [PubMed]
46. Ebrahimi, M.; Shaeri, M.H.; Naseri, R.; Gode, C. Equal channel angular extrusion for tube configuration of Al-Zn-Mg-Cu alloy. *Mater. Sci. Eng. A* **2018**, *731*, 569–576. [CrossRef]
47. Jing, X.; Lu, N.; Huang, J.; Zhang, P.; Zhang, Z. One-step hydrothermal synthesis of S-defect-controlled $ZnIn_2S_4$ microflowers with improved kinetics process of charge-carriers for photocatalytic H_2 evolution. *J. Energy Chem.* **2021**, *58*, 397–407. [CrossRef]
48. Ong, C.B.; Ng, L.Y.; Mohammad, A.W. A review of ZnO nanoparticles as solar photocatalysts: Synthesis, mechanisms and applications. *Renew. Sustain. Energy Rev.* **2018**, *81*, 536–551. [CrossRef]
49. Goktas, S.; Goktas, A. A comparative study on recent progress in efficient ZnO based nanocomposite and heterojunction photocatalysts: A review. *J. Alloys Compd.* **2021**, *863*, 158734. [CrossRef]
50. Habibi-Yangjeh, A.; Pirhashemi, M.; Ghosh, S. $ZnO/ZnBi_2O_4$ nanocomposites with p-n heterojunction as durable visible-light-activated photocatalysts for efficient removal of organic pollutants. *J. Alloys Compd.* **2020**, *826*, 154229. [CrossRef]
51. Attarilar, S.; Yang, J.; Ebrahimi, M.; Wang, Q.; Liu, J.; Tang, Y.; Yang, J. The Toxicity Phenomenon and the Related Occurrence in Metal and Metal Oxide Nanoparticles: A Brief Review From the Biomedical Perspective. *Front. Bioeng. Biotechnol.* **2020**, *8*, 822. [CrossRef]
52. Pirhashemi, M.; Habibi-Yangjeh, A.; Rahim Pouran, S. Review on the criteria anticipated for the fabrication of highly efficient ZnO-based visible-light-driven photocatalysts. *J. Ind. Eng. Chem.* **2018**, *62*, 1–25. [CrossRef]
53. Huang, H.; Liu, L.; Zhang, Y.; Tian, N. Novel $BiIO_4/BiVO_4$ composite photocatalyst with highly improved visible-light-induced photocatalytic performance for rhodamine B degradation and photocurrent generation. *RSC Adv.* **2015**, *5*, 1161–1167. [CrossRef]
54. Dong, D.; Yan, C.; Huang, J.; Lu, N.; Wu, P.; Wang, J.; Zhang, Z. An electron-donating strategy to guide the construction of MOF photocatalysts toward co-catalyst-free highly efficient photocatalytic H_2 evolution. *J. Mater. Chem. A* **2019**, *7*, 24180–24185. [CrossRef]
55. Dutta, V.; Sharma, S.; Raizada, P.; Thakur, V.K.; Khan, A.A.P.; Saini, V.; Asiri, A.M.; Singh, P. An overview on WO_3 based photocatalyst for environmental remediation. *J. Environ. Chem. Eng.* **2021**, *9*, 105018. [CrossRef]

56. Tachibana, Y.; Vayssieres, L.; Durrant, J.R. Artificial photosynthesis for solar water-splitting. *Nat. Photonics* **2012**, *6*, 511–518. [CrossRef]
57. Li, H.; Tu, W.; Zhou, Y.; Zou, Z. Z-Scheme Photocatalytic Systems for Promoting Photocatalytic Performance: Recent Progress and Future Challenges. *Adv. Sci.* **2016**, *3*, 1500389. [CrossRef] [PubMed]
58. Low, J.; Jiang, C.; Cheng, B.; Wageh, S.; Al-Ghamdi, A.A.; Yu, J. A Review of Direct Z-Scheme Photocatalysts. *Small Methods* **2017**, *1*, 1700080. [CrossRef]
59. Chen, S.; Hu, Y.; Jiang, X.; Meng, S.; Fu, X. Fabrication and characterization of novel Z-scheme photocatalyst WO_3/g-C_3N_4 with high efficient visible light photocatalytic activity. *Mater. Chem. Phys.* **2015**, *149–150*, 512–521. [CrossRef]
60. He, Y.; Zhang, L.; Wang, X.; Wu, Y.; Lin, H.; Zhao, L.; Weng, W.; Wan, H.; Fan, M. Enhanced photodegradation activity of methyl orange over Z-scheme type MoO_3–g-C_3N_4 composite under visible light irradiation. *RSC Adv.* **2014**, *4*, 13610–13619. [CrossRef]
61. Yu, J.; Wang, S.; Low, J.; Xiao, W. Enhanced photocatalytic performance of direct Z-scheme g-C_3N_4–TiO_2 photocatalysts for the decomposition of formaldehyde in air. *Phys. Chem. Chem. Phys.* **2013**, *15*, 16883. [CrossRef]
62. Bard, A.J. Photoelectrochemistry and heterogeneous photo-catalysis at semiconductors. *J. Photochem.* **1979**, *10*, 59–75. [CrossRef]
63. Katsumata, H.; Tachi, Y.; Suzuki, T.; Kaneco, S. Z-scheme photocatalytic hydrogen production over WO_3/g-C_3N_4 composite photocatalysts. *RSC Adv.* **2014**, *4*, 21405–21409. [CrossRef]
64. Chen, S.; Hu, Y.; Ji, L.; Jiang, X.; Fu, X. Preparation and characterization of direct Z-scheme photocatalyst Bi_2O_3/$NaNbO_3$ and its reaction mechanism. *Appl. Surf. Sci.* **2014**, *292*, 357–366. [CrossRef]
65. Tian, N.; Huang, H.; He, Y.; Guo, Y.; Zhang, T.; Zhang, Y. Mediator-free direct Z-scheme photocatalytic system: $BiVO_4$/g-C_3N_4 organic–inorganic hybrid photocatalyst with highly efficient visible-light-induced photocatalytic activity. *Dalt. Trans.* **2015**, *44*, 4297–4307. [CrossRef] [PubMed]
66. Zhang, Z.; Jiang, D.; Xing, C.; Chen, L.; Chen, M.; He, M. Novel AgI-decorated β-Bi_2O_3 nanosheet heterostructured Z-scheme photocatalysts for efficient degradation of organic pollutants with enhanced performance. *Dalt. Trans.* **2015**, *44*, 11582–11591. [CrossRef] [PubMed]
67. Zhou, H.; Wen, Z.; Liu, J.; Ke, J.; Duan, X.; Wang, S. Z-scheme plasmonic Ag decorated WO_3/Bi_2WO_6 hybrids for enhanced photocatalytic abatement of chlorinated-VOCs under solar light irradiation. *Appl. Catal. B Environ.* **2019**, *242*, 76–84. [CrossRef]
68. Tang, Q.-Y.; Chen, W.-F.; Lv, Y.-R.; Yang, S.-Y.; Xu, Y.-H. Z-scheme hierarchical Cu_2S/Bi_2WO_6 composites for improved photocatalytic activity of glyphosate degradation under visible light irradiation. *Sep. Purif. Technol.* **2020**, *236*, 116243. [CrossRef]
69. Li, Z.; Chen, M.; Zhang, Q.; Tao, D. Mechanochemical synthesis of a Z-scheme Bi_2WO_6/$CuBi_2O_4$ heterojunction and its visible-light photocatalytic degradation of ciprofloxacin. *J. Alloys Compd.* **2020**, *845*, 156291. [CrossRef]
70. Li, Q.; Lu, M.; Wang, W.; Zhao, W.; Chen, G.; Shi, H. Fabrication of 2D/2D g-C_3N_4/Au/Bi_2WO_6 Z-scheme photocatalyst with enhanced visible-light-driven photocatalytic activity. *Appl. Surf. Sci.* **2020**, *508*, 144182. [CrossRef]
71. Xu, Q.; Zhang, L.; Cheng, B.; Fan, J.; Yu, J. S-Scheme Heterojunction Photocatalyst. *Chem* **2020**, *6*, 1543–1559. [CrossRef]
72. Wang, J.; Zhang, Q.; Deng, F.; Luo, X.; Dionysiou, D.D. Rapid toxicity elimination of organic pollutants by the photocatalysis of environment-friendly and magnetically recoverable step-scheme $SnFe_2O_4$/$ZnFe_2O_4$ nano-heterojunctions. *Chem. Eng. J.* **2020**, *379*, 122264. [CrossRef]
73. Mei, F.; Dai, K.; Zhang, J.; Li, W.; Liang, C. Construction of Ag SPR-promoted step-scheme porous g-C_3N_4/Ag_3VO_4 heterojunction for improving photocatalytic activity. *Appl. Surf. Sci.* **2019**, *488*, 151–160. [CrossRef]
74. Jia, X.; Han, Q.; Zheng, M.; Bi, H. One pot milling route to fabricate step-scheme AgI/I-BiOAc photocatalyst: Energy band structure optimized by the formation of solid solution. *Appl. Surf. Sci.* **2019**, *489*, 409–419. [CrossRef]
75. Wang, R.; Shen, J.; Zhang, W.; Liu, Q.; Zhang, M.; Zulfiqar; Tang, H. Build-in electric field induced step-scheme TiO_2/$W_{18}O_{49}$ heterojunction for enhanced photocatalytic activity under visible-light irradiation. *Ceram. Int.* **2020**, *46*, 23–30. [CrossRef]
76. Hu, T.; Dai, K.; Zhang, J.; Zhu, G.; Liang, C. One-pot synthesis of step-scheme Bi_2S_3/porous g-C_3N_4 heterostructure for enhanced photocatalytic performance. *Mater. Lett.* **2019**, *257*, 126740. [CrossRef]
77. He, F.; Zhu, B.; Cheng, B.; Yu, J.; Ho, W.; Macyk, W. 2D/2D/0D TiO_2/C_3N_4/Ti_3C_2 MXene composite S-scheme photocatalyst with enhanced CO_2 reduction activity. *Appl. Catal. B Environ.* **2020**, *272*, 119006. [CrossRef]
78. Meng, A.; Cheng, B.; Tan, H.; Fan, J.; Su, C.; Yu, J. TiO_2/polydopamine S-scheme heterojunction photocatalyst with enhanced CO_2-reduction selectivity. *Appl. Catal. B Environ.* **2021**, *289*, 120039. [CrossRef]
79. Kumar, R.; Raizada, P.; Verma, N.; Hosseini-Bandegharaei, A.; Thakur, V.K.; Van Le, Q.; Nguyen, V.-H.; Selvasembian, R.; Singh, P. Recent advances on water disinfection using bismuth based modified photocatalysts: Strategies and challenges. *J. Clean. Prod.* **2021**, *297*, 126617. [CrossRef]
80. Enesca, A.; Andronic, L. Photocatalytic Activity of S-Scheme Heterostructure for Hydrogen Production and Organic Pollutant Removal: A Mini-Review. *Nanomaterials* **2021**, *11*, 871. [CrossRef]
81. Fu, J.; Xu, Q.; Low, J.; Jiang, C.; Yu, J. Ultrathin 2D/2D WO_3/g-C_3N_4 step-scheme H_2-production photocatalyst. *Appl. Catal. B Environ.* **2019**, *243*, 556–565. [CrossRef]
82. Mohamed, R.M.; Ismail, A.A. Photocatalytic reduction and removal of mercury ions over mesoporous CuO/ZnO S-scheme heterojunction photocatalyst. *Ceram. Int.* **2021**, *47*, 9659–9667. [CrossRef]
83. Jin, Z.; Zhang, L.; Wang, G.; Li, Y.; Wang, Y. Graphdiyne formed a novel CuI-GD/g-C_3N_4 S-scheme heterojunction composite for efficient photocatalytic hydrogen evolution. *Sustain. Energy Fuels* **2020**, *4*, 5088–5101. [CrossRef]

84. Xia, P.; Cao, S.; Zhu, B.; Liu, M.; Shi, M.; Yu, J.; Zhang, Y. Designing a 0D/2D S-Scheme Heterojunction over Polymeric Carbon Nitride for Visible-Light Photocatalytic Inactivation of Bacteria. *Angew. Chemie Int. Ed.* **2020**, *59*, 5218–5225. [CrossRef] [PubMed]
85. He, F.; Meng, A.; Cheng, B.; Ho, W.; Yu, J. Enhanced photocatalytic H_2-production activity of WO_3/TiO_2 step-scheme heterojunction by graphene modification. *Chin. J. Catal.* **2020**, *41*, 9–20. [CrossRef]
86. Deng, H.; Fei, X.; Yang, Y.; Fan, J.; Yu, J.; Cheng, B.; Zhang, L. S-scheme heterojunction based on p-type $ZnMn_2O_4$ and n-type ZnO with improved photocatalytic CO_2 reduction activity. *Chem. Eng. J.* **2021**, *409*, 127377. [CrossRef]
87. Brabec, C.J.; Heeney, M.; McCulloch, I.; Nelson, J. Influence of blend microstructure on bulk heterojunction organic photovoltaic performance. *Chem. Soc. Rev.* **2011**, *40*, 1185–1199. [CrossRef]
88. Vandewal, K.; Himmelberger, S.; Salleo, A. Structural Factors That Affect the Performance of Organic Bulk Heterojunction Solar Cells. *Macromolecules* **2013**, *46*, 6379–6387. [CrossRef]
89. Zeng, P.; Zhang, X.; Zhang, X.; Chai, B.; Peng, T. Efficient photocatalytic hydrogen production over Ni@C/TiO_2 nanocomposite under visible light irradiation. *Chem. Phys. Lett.* **2011**, *503*, 262–265. [CrossRef]
90. Xiang, Q.; Yu, J.; Jaroniec, M. Enhanced photocatalytic H2-production activity of graphene-modified titania nanosheets. *Nanoscale* **2011**, *3*, 3670. [CrossRef]
91. Chai, B.; Peng, T.; Zeng, P.; Mao, J. Synthesis of floriated In_2S_3 decorated with TiO_2 nanoparticles for efficient photocatalytic hydrogen production under visible light. *J. Mater. Chem.* **2011**, *21*, 14587. [CrossRef]
92. Bian, Z.; Tachikawa, T.; Zhang, P.; Fujitsuka, M.; Majima, T. Au/TiO_2 Superstructure-Based Plasmonic Photocatalysts Exhibiting Efficient Charge Separation and Unprecedented Activity. *J. Am. Chem. Soc.* **2014**, *136*, 458–465. [CrossRef]
93. Martha, S.; Das, D.P.; Biswal, N.; Parida, K.M. Facile synthesis of visible light responsive V_2O_5/N,S–TiO_2 composite photocatalyst: Enhanced hydrogen production and phenol degradation. *J. Mater. Chem.* **2012**, *22*, 10695. [CrossRef]
94. Jang, J.S.; Hong, S.J.; Kim, J.Y.; Lee, J.S. Heterojunction photocatalyst $TiO_2/AgGaS_2$ for hydrogen production from water under visible light. *Chem. Phys. Lett.* **2009**, *475*, 78–81. [CrossRef]
95. Zhu, S.; Yao, F.; Yin, C.; Li, Y.; Peng, W.; Ma, J.; Zhang, D. Fe_2O_3/TiO_2 photocatalyst of hierarchical structure for H_2 production from water under visible light irradiation. *Microporous Mesoporous Mater.* **2014**, *190*, 10–16. [CrossRef]
96. Amirav, L.; Alivisatos, A.P. Photocatalytic Hydrogen Production with Tunable Nanorod Heterostructures. *J. Phys. Chem. Lett.* **2010**, *1*, 1051–1054. [CrossRef]
97. Lu, X.-H.; Xie, S.-L.; Zhai, T.; Zhao, Y.-F.; Zhang, P.; Zhang, Y.-L.; Tong, Y.-X. Monodisperse CeO_2/CdS heterostructured spheres: One-pot synthesis and enhanced photocatalytic hydrogen activity. *RSC Adv.* **2011**, *1*, 1207. [CrossRef]
98. Shen, Z.; Chen, G.; Wang, Q.; Yu, Y.; Zhou, C.; Wang, Y. Sonochemistry synthesis and enhanced photocatalytic H_2-production activity of nanocrystals embedded in CdS/ZnS/In_2S_3 microspheres. *Nanoscale* **2012**, *4*, 2010. [CrossRef] [PubMed]
99. Chang, K.; Mei, Z.; Wang, T.; Kang, Q.; Ouyang, S.; Ye, J. MoS_2/Graphene Cocatalyst for Efficient Photocatalytic H_2 Evolution under Visible Light Irradiation. *ACS Nano* **2014**, *8*, 7078–7087. [CrossRef] [PubMed]
100. Hu, T.; Dai, K.; Zhang, J.; Chen, S. Noble-metal-free Ni_2P modified step-scheme $SnNb_2O_6$/CdS-diethylenetriamine for photocatalytic hydrogen production under broadband light irradiation. *Appl. Catal. B Environ.* **2020**, *269*, 118844. [CrossRef]
101. Zhang, X.; Yu, L.; Zhuang, C.; Peng, T.; Li, R.; Li, X. Highly Asymmetric Phthalocyanine as a Sensitizer of Graphitic Carbon Nitride for Extremely Efficient Photocatalytic H_2 Production under Near-Infrared Light. *ACS Catal.* **2014**, *4*, 162–170. [CrossRef]
102. Chen, J.; Shen, S.; Guo, P.; Wu, P.; Guo, L. Spatial engineering of photo-active sites on g-C_3N_4 for efficient solar hydrogen generation. *J. Mater. Chem. A* **2014**, *2*, 4605. [CrossRef]
103. Kang, H.W.; Lim, S.N.; Song, D.; Park, S. Bin Organic-inorganic composite of g-C_3N_4–$SrTiO_3$:Rh photocatalyst for improved H_2 evolution under visible light irradiation. *Int. J. Hydrogen Energy* **2012**, *37*, 11602–11610. [CrossRef]
104. Chai, B.; Peng, T.; Mao, J.; Li, K.; Zan, L. Graphitic carbon nitride (g-C_3N_4)–Pt-TiO_2 nanocomposite as an efficient photocatalyst for hydrogen production under visible light irradiation. *Phys. Chem. Chem. Phys.* **2012**, *14*, 16745. [CrossRef] [PubMed]
105. Kim, H.N.; Kim, T.W.; Kim, I.Y.; Hwang, S.-J. Cocatalyst-Free Photocatalysts for Efficient Visible-Light-Induced H_2 Production: Porous Assemblies of CdS Quantum Dots and Layered Titanate Nanosheets. *Adv. Funct. Mater.* **2011**, *21*, 3111–3118. [CrossRef]
106. Oskoui, M.S.; Khatamian, M.; Haghighi, M.; Yavari, A. Photocatalytic hydrogen evolution from water over chromosilicate-based catalysts. *RSC Adv.* **2014**, *4*, 19569. [CrossRef]
107. Fang, J.; Xu, L.; Zhang, Z.; Yuan, Y.; Cao, S.; Wang, Z.; Yin, L.; Liao, Y.; Xue, C. Au@TiO_2–CdS Ternary Nanostructures for Efficient Visible-Light-Driven Hydrogen Generation. *ACS Appl. Mater. Interfaces* **2013**, *5*, 8088–8092. [CrossRef]
108. Bahadoran, A.; Masudy-Panah, S.; De Lile, J.R.; Li, J.; Gu, J.; Sadeghi, B.; Ramakrishna, S.; Liu, Q. Novel 0D/1D $ZnBi_2O_4$/ZnO S-scheme photocatalyst for hydrogen production and BPA removal. *Int. J. Hydrogen Energy* **2021**, *46*, 24094–24106. [CrossRef]
109. Lin, W.; Zhang, S.; Wang, D.; Zhang, C.; Sun, D. Ultrasound-assisted synthesis of high-efficiency Ag_3PO_4/CeO_2 heterojunction photocatalyst. *Ceram. Int.* **2015**, *41*, 8956–8963. [CrossRef]
110. Tho, N.T.M.; Khanh, D.N.N.; Thang, N.Q.; Lee, Y.-I.; Phuong, N.T.K. Novel reduced graphene oxide/$ZnBi_2O_4$ hybrid photocatalyst for visible light degradation of 2,4-dichlorophenoxyacetic acid. *Environ. Sci. Pollut. Res.* **2020**, *27*, 11127–11137. [CrossRef]
111. Selvi, S.; Rajendran, R.; Jayamani, N. Hydrothermal fabrication and characterization of novel $CeO_2/PbWO_4$ nanocomposite for enhanced visible-light photocatalytic performance. *Appl. Water Sci.* **2021**, *11*, 93. [CrossRef]
112. Li, X.; Yao, C.; Lu, X.; Hu, Z.; Yin, Y.; Ni, C. Halloysite–CeO_2–AgBr nanocomposite for solar light photodegradation of methyl orange. *Appl. Clay Sci.* **2015**, *104*, 74–80. [CrossRef]

113. Zhakeyev, A.; Wang, P.; Zhang, L.; Shu, W.; Wang, H.; Xuan, J. Additive Manufacturing: Unlocking the Evolution of Energy Materials. *Adv. Sci.* **2017**, *4*, 1700187. [CrossRef]
114. Attarilar, S.; Djavanroodi, F.; Ebrahimi, M.; Al-Fadhalah, K.J.; Wang, L.; Mozafari, M. Hierarchical Microstructure Tailoring of Pure Titanium for Enhancing Cellular Response at Tissue-Implant Interface. *J. Biomed. Nanotechnol.* **2021**, *17*, 115–130. [CrossRef] [PubMed]
115. Zhang, Y.; Attarilar, S.; Wang, L.; Lu, W.; Yang, J.; Fu, Y. A Review on Design and Mechanical Properties of Additively Manufactured NiTi Implants for Orthopedic Applications. *Int. J. Bioprint.* **2021**, *7*, 340. [CrossRef] [PubMed]
116. Sun, L.; Zhuang, Y.; Yuan, Y.; Zhan, W.; Wang, X.; Han, X.; Zhao, Y. Nitrogen-Doped Carbon-Coated CuO-In_2O_3 p–n Heterojunction for Remarkable Photocatalytic Hydrogen Evolution. *Adv. Energy Mater.* **2019**, *9*, 1902839. [CrossRef]
117. Nguyen, V.-H.; Mousavi, M.; Ghasemi, J.B.; Van Le, Q.; Delbari, S.A.; Sabahi Namini, A.; Shahedi Asl, M.; Shokouhimehr, M.; Mohammadi, M. Novel p–n Heterojunction Nanocomposite: TiO_2 QDs/$ZnBi_2O_4$ Photocatalyst with Considerably Enhanced Photocatalytic Activity under Visible-Light Irradiation. *J. Phys. Chem. C* **2020**, *124*, 27519–27528. [CrossRef]
118. Attarilar, S.; Ebrahimi, M.; Djavanroodi, F.; Fu, Y.; Wang, L.; Yang, J. 3D Printing Technologies in Metallic Implants: A Thematic Review on the Techniques and Procedures. *Int. J. Bioprint.* **2021**, *7*, 306. [CrossRef]
119. Gellé, A.; Jin, T.; de la Garza, L.; Price, G.D.; Besteiro, L.V.; Moores, A. Applications of Plasmon-Enhanced Nanocatalysis to Organic Transformations. *Chem. Rev.* **2020**, *120*, 986–1041. [CrossRef]
120. Linic, S.; Chavez, S.; Elias, R. Flow and extraction of energy and charge carriers in hybrid plasmonic nanostructures. *Nat. Mater.* **2021**, *20*, 916–924. [CrossRef]
121. Jiang, X.; Huang, J.; Bi, Z.; Ni, W.; Gurzadyan, G.; Zhu, Y.; Zhang, Z. Plasmonic Active "Hot Spots"-Confined Photocatalytic CO_2 Reduction with High Selectivity for CH_4 Production. *Adv. Mater.* **2022**, *34*, 2109330. [CrossRef]